

Neutrino oscillation measurements with JUNO in the presence of scalar NSI

Aman Gupta,^{1,2,*} Debasish Majumdar,^{1,2,†} and Suprabh Prakash^{3,4,‡}

¹*Theory Division, Saha Institute of Nuclear Physics,*

1/AF, Bidhannagar, Kolkata 700064, India

²*Homi Bhabha National Institute, Anushakti Nagar, Mumbai 400094, India*

³*The Institute of Mathematical Sciences, C.I.T. Campus, Taramani, Chennai 600113, India*

⁴*Division of Physics, School of Advanced Sciences,*

Vellore Institute of Technology Chennai Campus, Chennai 600127, India

Determination of neutrino mass ordering and precision measurement of neutrino oscillation parameters are the foremost goals of the JUNO experiment. Here, we explore the capability of JUNO experiment to constrain the scalar non-standard interactions (sNSI). sNSI appears as a correction to the neutrino mass term in the Hamiltonian. Our results show that JUNO can put very stringent constraints on sNSI, particularly for the case of inverted mass ordering. We also check JUNO's capability to determine mass ordering in the presence of sNSI and conclude that the possibility to confuse normal (inverted) mass ordering in the standard scenario (when there is no sNSI) with inverted (normal) ordering in the presence of sNSI exists only at the 3σ confidence level and above. Finally, we also comment on the precision measurements of $\sin^2 \theta_{12}$, Δm_{21}^2 and Δm_{31}^2 in the presence of sNSI. We find that the 1σ -allowed uncertainty in each of these oscillation parameters depends on the choice of mass ordering, sNSI and m_{lightest} , wherein a deterioration from a few percent in the case of standard interactions to $\sim 13\%$ in the case of sNSI is possible.

* aman.gupta@saha.ac.in(ORCID:0000-0002-7247-2424)

† debsish.majumdar@saha.ac.in

‡ suprabh.prakash@vit.ac.in(ORCID:0000-0002-1529-4588)

I. INTRODUCTION

The discovery of neutrino flavour oscillations [1–3] implies that neutrinos are massive which is one of the few observational indications in particle physics with regard to the physics beyond the Standard Model (BSM). From the evolution of the Universe to matter-antimatter asymmetry in the Universe, neutrinos play very important role in cosmology and several aspects of elementary particle physics. At present, neutrino oscillation physics has entered in to the precision era. In the standard three flavor paradigm neutrino oscillation is governed by two mass squared differences: Δm_{21}^2 and Δm_{31}^2 , three leptonic mixing angles: θ_{23}, θ_{13} and θ_{12} and probably a CP-violating phase δ_{CP} . Several experiments searching for the solar, reactor, atmospheric and accelerator neutrinos have measured these neutrino oscillation parameters with great precision [4–7]. However, at the moment there are three principal unknowns in oscillation physics namely the octant of θ_{23} , the existence and the measure of Dirac CP phase, δ_{CP} and the neutrino mass hierarchy or the ordering of neutrino masses (m_1, m_2, m_3). In addition to this, the absolute masses and Dirac or Majorana nature of neutrinos are two fundamental problems in neutrino physics, which are yet to be answered.

The data and their analysis from the various solar neutrino experiments [2, 8–12] suggest that $\Delta m_{21}^2 = m_2^2 - m_1^2 > 0$, which means $m_2 > m_1$. However, the ordering between m_1 and m_3 is yet to be determined. If $m_3 > m_1$ then the sign of $\Delta m_{31}^2 = m_3^2 - m_1^2$ is +ve which is referred to as the normal ordering (NO) for neutrino masses whereas, in case, when $m_3 < m_1$, Δm_{31}^2 is -ve giving rise to the inverted ordering (IO) of neutrino masses. It is worth mentioning here that combining all the available data from accelerator-based experiments (such as T2K [13, 14] and NO ν A [15, 16]) to the experiments targeting atmospheric neutrinos (such as Super-Kamiokande [17] and IceCube [18]), the global fits [5] exhibit a slight preference for normal mass ordering over the inverted one. Solving the puzzle of neutrino mass hierarchy to a significant confidence level is one of the primary goals of future accelerator based experiments such as DUNE [19], T2HK [20], and T2HKK [21] but the results from these experiments may be available by 2030 or later. Therefore, we need some alternative experiments such as atmospheric based KM3NeT/ORCA [22] and PINGU [23] and reactor based experiments such as JUNO [24, 25] which are aiming to address the neutrino mass ordering (NMO) problem and serve as complementary to the accelerator one. Currently JUNO detector is under construction and expecting first data in 2023. This makes JUNO experiment at the front line of determining NMO.

Despite the fact that three flavour neutrino frame-work can successfully explain most of the

available oscillation data, there are several new physics scenarios [26, 27] arise as a consequence of BSM physics. The non-standard interaction [28, 29] (NSI) of neutrinos with ordinary matter is one of those new physics cases which may significantly modify the neutrino oscillation and affect the mass hierarchy sensitivity of such experiments.

Therefore it is important to study the effects of NSI in NMO sensitivity of JUNO detector. NSIs can be further divided into two parts namely vector NSI and scalar NSI. For vector NSI new interactions are mediated by vector boson and can be parameterized with vector current akin to the ordinary matter effect [28] but with unknown couplings, and for the scalar NSI, on the other hand, neutrinos can couple to the scalar fields giving rise to correction to the neutrino mass term [30]. The impact of vector NSI which acts like a new term to the standard matter potential has been discussed with great details in [31–37]. The mass ordering sensitivities of T2K, NO ν A and other long-baseline (LBL) neutrino oscillation experiments are considerably affected by the presence of vector NSI and these are conferred in [32, 38–40]. In the Ref. [41], the authors have shown that the mass ordering sensitivity of JUNO may get weaken if neutrino decoherence as new physics is included in the standard three flavour model. Recently there are also growing interest in exploring the effects of scalar NSI in neutrino oscillation experiments [30, 42–46]. There are attempts to explain solar neutrino data from Borexino experiment [47] within the oscillation formulation that includes scalar NSI [30]. Some constraints on scalar NSI parameters are obtained from big bang nucleosynthesis [48] and also studies are made on these elements using various astrophysical and cosmological constraints [33]. In the reference [49], the authors have discussed how to discriminate these two effects in the context of DUNE [19] experiment.

In this work, we have studied for the first time, the impact of scalar NSI elements on NMO sensitivity at JUNO experiment, a medium baseline reactor (anti)neutrino detector. Unlike LBL experiments, JUNO will utilise the electron antineutrino survival probability (\bar{P}_{ee}) spectra to distinguish the normal mass ordering from the inverted one. If scalar NSI exists in nature, we have found that in the presence of scalar NSI the electron (anti)neutrino disappearance probability pattern changes significantly and in a different manner for NO and IO. In addition, we also demonstrate that this survival probability depends upon the Dirac CP phase δ_{CP} and atmospheric mixing angle θ_{23} , if scalar NSI is included in the Hamiltonian for neutrino oscillation.

The paper is structured as follows. In section II, we briefly discuss about the vector and scalar NSIs and their distinct nature. In section III, provide a theoretical formalism of scalar NSI and compute the matrix elements of effective Hamiltonian for neutrino propagation. Later in section IV, we drive the analytical expressions for modified mixing angles and mass-squared

differences considering η_{ee} only as scalar NSI parameter. Subsequently, we present the simple probability formula to understand the results. In section V, we provide a brief account of electron (anti)neutrino survival probability to exhibit its physics capability in determining the NMO at medium baseline reactor (anti)neutrino experiments such as JUNO. In section VII, we talk about JUNO experiments and simulation techniques used in this analysis. In section VIII, we furnish the calculations and the results of our analysis. Finally in section IX, we summarize the work with some discussions.

II. VECTOR AND SCALAR NSI

The non-standard neutrino interaction with matter is one of the most widely explored BSM physics in neutrino oscillation. In this section, we describe the theoretical formalism of such new interactions of neutrinos with matter namely, vector and scalar non-standard interactions. We also try to explain the different nature of the above two types of non-standard interactions.

Vector NSI

The coherent forward scattering off neutrinos with matter leads to the matter effect in neutrino oscillation which was first proposed by L. Wolfenstein [50]. One of the important features of this paper is that it introduces possibility of new non-standard interactions (NSIs) of neutrinos with matter via vector type mediator. The vector NSI can be of two types namely Charged Current (CC) NSI and Neutral Current (NC) NSI. It is to be noted that the vector CC NSI affects the production and detection channels of neutrinos while the NC part of vector NSI modifies the propagation of neutrinos through material medium just as the matter effect influences the new-propagation through matter [51–53]. The effective Lagrangian corresponding to the neutral current vector NSI ¹ be written using the dimensional six operators as [35, 54],

$$\mathcal{L}_{\text{NSI}}^{\text{NCvector}} = -2\sqrt{2}G_F \sum_{\alpha,\beta,f} \epsilon_{\alpha\beta}^f (\bar{\nu}_\alpha \gamma^\mu P_L \nu_\beta) (\bar{f} \gamma_\mu P_C f), \quad (1)$$

where G_F is the Fermi coupling constant, and $C = L, R$ corresponding to the left and right chiral projection operators (P_L and P_R), respectively. The strength of NSI is parameterized by the dimensionless coefficients $\epsilon_{\alpha\beta}^f$ where f denotes the first generation SM fermions (e, u or d) and α, β

¹ For detailed review on vector type NSI, kindly refer to [29, 32]

represent lepton flavours e, μ or τ . The effective NSI parameters $\epsilon_{\alpha\beta}$ relevant in neutrino oscillation experiments are related to the coefficient $\epsilon_{\alpha\beta}^f$ as

$$\epsilon_{\alpha\beta} = \sum_{f=e,u,d} \epsilon_{\alpha\beta}^f \frac{N_f}{N_e}, \quad (2)$$

where N_f is the number density of first generation fermions $f \in e, u, d$. The effective Hamiltonian in presence of such non-standard interactions takes the form

$$\mathcal{H}_V^{eff} = \frac{1}{2E} \left[\mathcal{M} \mathcal{M}^\dagger + 2EV_{CC} \begin{pmatrix} 1 + \epsilon_{ee} & \epsilon_{e\mu} & \epsilon_{e\tau} \\ \epsilon_{e\mu}^* & \epsilon_{\mu\mu} & \epsilon_{\mu\tau} \\ \epsilon_{e\tau}^* & \epsilon_{\mu\tau}^* & \epsilon_{\tau\tau} \end{pmatrix} \right], \quad (3)$$

where $\mathcal{M} = U \begin{pmatrix} m_1 & 0 & 0 \\ 0 & m_2 & 0 \\ 0 & 0 & m_3 \end{pmatrix} U^\dagger$ is the neutrino mass matrix in flavour basis and $V_{CC} = \pm\sqrt{2}G_F N_e$ is the matter potential term due to the CC interactions of neutrinos with matter. Here, U is the standard 3×3 Pontecorvo-Maki-Nakagawa-Sakata (PMNS) mixing matrix [55–58], N_e is the electron number density of neutrino propagation medium and E is the neutrino energy. The fact that the Hamiltonian in Eq. 8 should be Hermitian implies that the diagonal NSI elements are real while the off-diagonal elements are complex in general with phase $\epsilon_{\alpha\beta}$ and can be written as $\epsilon_{\alpha\beta} = |\epsilon_{\alpha\beta}|e^{i\phi_{\alpha\beta}}$. The neutrino masses corresponding to the three neutrino mass eigen states ν_1, ν_2 and ν_3 are denoted by m_1, m_2 and m_3 , respectively. It should be noted from Eq. 8 that the vector NSI appears as an additional potential term to the Hamiltonian along with the usual matter potential. Since the matter potential involves the term $2EV_{CC}$, its effect will be large for higher neutrino energies and larger matter density making it significant for Long Baseline (LBL) neutrino experiments. Numerous phenomenological studies have already been made in these directions [5, 59–62]. The vector NSI parameters can be well constrained by LBL experiments while matter effect plays an important role.

Scalar NSI

Non-standard interactions for neutrinos may also proceed via coupling to a scalar field. Such interactions are mediated by scalars. In case a scalar field ϕ with mass m_ϕ that couples with neutrinos via NSI, the effective Lagrangian for such a scalar NSI can be written in terms of dimension

six operators as

$$\mathcal{L}_{\text{NSI}}^{\text{eff scalar}} = \frac{y_f Y_{\alpha\beta}}{m_\phi^2} [\bar{\nu}_\alpha(p_3) \nu_\beta(p_2)] [\bar{f}(p_1) f(p_4)], \quad (4)$$

where y_f and $Y_{\alpha\beta}$ are the Yukawa couplings of neutrinos with the scalar field ϕ and matter fermions $f \in \{e, u, d\}$, respectively. The presence of Yukawa terms in the above Lagrangian in Eq. 4 ensure that it can not be written as vector type currents [52, 53]. Clearly, it is no more a matter potential term as we have seen in case of vector type NSI. The corresponding Dirac equation in presence of scalar NSI can be written in the following form

$$\bar{\nu}_\beta \left[i\partial_\mu \gamma^\mu + \left(\sum_f N_f y_f Y_{\alpha\beta} \right) \right] \nu_\alpha = 0, \quad (5)$$

where N_f is the number density of ambient fermions f and $M_{\beta\alpha}$ is the mass matrix for neutrinos. The effective Hamiltonian for neutrino oscillations in presence of scalar NSI takes the form [44, 63, 64]

$$\mathcal{H}_S^{\text{eff}} \approx \frac{1}{2E} \left[(\mathcal{M} + \delta M)(\mathcal{M} + \delta M)^\dagger + 2EV_{CC} \begin{pmatrix} 1 & 0 & 0 \\ 0 & 0 & 0 \\ 0 & 0 & 0 \end{pmatrix} \right], \quad (6)$$

where $\delta M \equiv \sum_f \frac{N_f y_f Y_{\alpha\beta}}{m_\phi^2}$ is the contribution due the scalar NSI. From Eqs. 5 and 6, it is evident that the effect of scalar mediated NSI is to modify the neutrino mass matrix and unlike the vector NSI case which modifies the effective matter potential, the scalar NSI appears as the correction to the mass term in the Hamiltonian. In order to study the effect of δM in neutrino oscillation, it is parameterized as [42, 47]

$$\delta M \equiv \sqrt{|\Delta m_{31}^2|} \begin{pmatrix} \eta_{ee} & \eta_{e\mu} & \eta_{e\tau} \\ \eta_{e\mu}^* & \eta_{\mu\mu} & \eta_{\mu\tau} \\ \eta_{e\tau}^* & \eta_{\mu\tau}^* & \eta_{\tau\tau} \end{pmatrix}, \quad (7)$$

where $\eta_{\alpha\beta}$ represents the strength of scalar NSI. Assuming the real scalar fields, the hermiticity of the effective Hamiltonian (Eq. 6) requires the diagonal elements of the scalar NSI matrix to be real while the non-diagonal parameters can be complex.

One of the intriguing highlights of scalar NSI is that the oscillation probabilities, as we will see later in the upcoming sections, do depend upon the absolute neutrino masses. This feature is absent in the cases of the standard interactions (SI) and vector NSI where oscillation probabilities

are only sensitive to the mass-squared differences. Consequently, this scalar NSI model offers, theoretically, to look for the absolute neutrino masses in neutrino oscillation. Moreover, this model is independent of choice of neutrino energy and hence can be probed in oscillation experiments of all energy ranges. We would also like to emphasize that unlike the vector NSI case where either of the neutrino energy or the matter effects should be large enough, the effect of scalar NSI is significant even in vacuum and so can be tested in such experiments where matter effects are negligible, such as JUNO.

In the present work, for a better understanding of scalar NSI we only consider the diagonal NSI parameters to be non-zero and moreover one NSI parameter at a time while keeping the remaining NSI elements to be equal to zero.

III. FORMALISM

In this section, we compute the expressions for the effective Hamiltonian in vacuum considering only diagonal scalar NSI parameters. The off-diagonal NSI elements are assumed to be zero. It should be noted that in the present analysis we neglect the matter effect which is a very good approximation for JUNO experiment. The effective vacuum Hamiltonian in the flavour basis including the scalar NSI can be written as [44, 63, 64]

$$\mathcal{H}_S^{eff} \approx \frac{1}{2E} \left[(\mathcal{M} + \delta M)(\mathcal{M} + \delta M)^\dagger \right]. \quad (8)$$

We can write the neutrino mass matrix \mathcal{M} in flavour basis as

$$\mathcal{M} = U_\nu \begin{pmatrix} m_1 & 0 & 0 \\ 0 & m_2 & 0 \\ 0 & 0 & m_3 \end{pmatrix} U_\nu^\dagger = \begin{pmatrix} \mathcal{M}_{11} & \mathcal{M}_{12} & \mathcal{M}_{13} \\ \mathcal{M}_{21} & \mathcal{M}_{22} & \mathcal{M}_{23} \\ \mathcal{M}_{31} & \mathcal{M}_{32} & \mathcal{M}_{33} \end{pmatrix} = \mathcal{M}^\dagger, \quad (9)$$

with

$$\begin{aligned}
\mathcal{M}_{11} &= c_{12}^2 c_{13}^3 m_1 + c_{13}^2 s_{12}^2 m_2 + m_3 s_{13}^2 \\
\mathcal{M}_{12} &= -c_{13} [(m_1 - m_2) s_{12} c_{12} c_{23} + s_{13} s_{23} e^{-i\delta_{CP}} (c_{12}^2 m_1 - m_3 + s_{12}^2 m_2)] \\
\mathcal{M}_{13} &= -c_{13} [(m_2 - m_1) s_{12} c_{12} s_{23} + s_{13} c_{23} e^{-i\delta_{CP}} (c_{12}^2 m_1 - m_3 + s_{12}^2 m_2)] \\
\mathcal{M}_{21} &= \mathcal{M}_{12}^* \\
\mathcal{M}_{22} &= m_1 s_{12}^2 c_{23}^2 + m_3 s_{23}^2 c_{13}^2 + m_2 s_{12}^2 s_{13}^2 s_{23}^2 + c_{12}^2 (m_2 c_{23}^2 + m_1 s_{13}^2 s_{23}^2) \\
&\quad + 2s_{12} c_{12} s_{23} c_{23} s_{13} (m_1 - m_2) \cos \delta_{CP} \\
\mathcal{M}_{23} &= s_{23} c_{23} [m_3 c_{13}^2 + c_{12}^2 (-m_2 + m_1 s_{13}^2) + s_{12}^2 (-m_1 + m_2 s_{13}^2)] \\
&\quad + c_{12} (m_1 - m_2) s_{13}^2 (c_{23}^2 e^{-i\delta_{CP}} - s_{23}^2 e^{i\delta_{CP}}) \\
\mathcal{M}_{31} &= \mathcal{M}_{13}^* \\
\mathcal{M}_{32} &= \mathcal{M}_{23}^* \\
\mathcal{M}_{33} &= m_3 c_{13}^2 c_{23}^2 + m_1 c_{12}^2 c_{23}^2 s_{13}^2 + m_2 s_{12}^2 s_{13}^2 c_{23}^2 + m_2 s_{23}^2 c_{12}^2 + m_1 s_{12}^2 s_{23}^2 \\
&\quad - 2s_{12} c_{12} s_{23} c_{23} s_{13} (m_1 - m_2) \cos \delta_{CP},
\end{aligned} \tag{10}$$

From Eq. 8, the simplified form of the effective Hamiltonian in vacuum including scalar NSI can be approximated as

$$\mathcal{H}_S^{eff} \approx \Delta_{31} \left[U_\nu \begin{pmatrix} 0 & 0 & 0 \\ 0 & \alpha & 0 \\ 0 & 0 & 1 \end{pmatrix} U_\nu^\dagger + \frac{1}{\Delta m_{31}^2} (\mathcal{M} \delta M^\dagger + \mathcal{M}^\dagger \delta M) \right], \tag{11}$$

where $\alpha = \frac{\Delta m_{21}^2}{\Delta m_{31}^2}$ and $\Delta_{31} = \frac{\Delta m_{31}^2}{2E}$. Note here that we have neglected the term δM^2 in above expression which is ~ 1000 times small compared to other terms.

If we define $\tilde{\mathcal{H}} = \frac{1}{\Delta m_{31}^2} [\mathcal{M} \delta M^\dagger + \mathcal{M}^\dagger \delta M] = \begin{pmatrix} h_{11} & h_{12} & h_{13} \\ h_{12}^* & h_{22} & h_{23} \\ h_{13}^* & h_{23}^* & h_{33} \end{pmatrix}$, then one can rewrite the elements

of effective matrix elements as

$$\begin{aligned}
\mathcal{H}_S^{eff11} &= \Delta_{31}(s_{13}^2 + \alpha s_{12}^2 c_{13}^2 + h_{11}) \\
\mathcal{H}_S^{eff12} &= \frac{\Delta_{31}}{2} [\sin 2\theta_{13}(1 - \alpha s_{12}^2) s_{23} e^{-i\delta_{CP}} + \alpha c_{13} c_{23} \sin 2\theta_{12} + 2h_{12}] \\
\mathcal{H}_S^{eff13} &= \frac{\Delta_{31}}{2} [\sin 2\theta_{13}(1 - \alpha s_{12}^2) c_{23} e^{-i\delta_{CP}} - \alpha \sin 2\theta_{12} c_{13} s_{23} + 2h_{13}] \\
\mathcal{H}_S^{eff22} &= \Delta_{31} [c_{13}^2 s_{23}^2 + \alpha c_{12}^2 c_{23}^2 + \alpha s_{12}^2 s_{13}^2 s_{23}^2 - \alpha s_{12} c_{12} s_{23} c_{23} s_{13} (e^{-i\delta_{CP}} + e^{i\delta_{CP}}) + h_{22}] \\
\mathcal{H}_S^{eff23} &= \frac{\Delta_{31}}{2} [\sin 2\theta_{23} c_{13}^2 + \alpha \sin 2\theta_{23} (s_{12}^2 s_{13}^2 - c_{12}^2) + \alpha \sin 2\theta_{12} s_{13} (s_{23}^2 e^{i\delta_{CP}} - c_{23}^2 e^{-i\delta_{CP}}) + 2h_{23}] \\
\mathcal{H}_S^{eff33} &= \Delta_{31} [c_{13}^2 c_{23}^2 + \alpha c_{12}^2 s_{23}^2 + \alpha s_{12}^2 s_{13}^2 c_{23}^2 + \alpha s_{12} c_{12} s_{23} c_{23} s_{13} (e^{-i\delta_{CP}} + e^{i\delta_{CP}}) + h_{33}], \quad (12)
\end{aligned}$$

with

$$\begin{aligned}
h_{11} &= 2r\eta_{ee} [c_{13}^2(m_1 c_{12}^2 + m_2 s_{12}^2) + m_3 s_{13}^2] \\
h_{12} &= c_{13}r(\eta_{ee} + \eta_{\mu\mu}) [-s_{12}c_{12}c_{23}d + s_{13}s_{23}e^{-i\delta_{CP}}(-m_1 c_{12}^2 + m_3 - m_2 s_{12}^2)] \\
h_{13} &= c_{13}r(\eta_{ee} + \eta_{\tau\tau}) [s_{12}c_{12}s_{23}d + s_{13}c_{23}e^{-i\delta_{CP}}(-m_1 c_{12}^2 + m_3 - m_2 s_{12}^2)] \\
h_{22} &= 2r\eta_{\mu\mu} [c_{23}^2(m_1 s_{12}^2 + m_2 c_{12}^2) + s_{23}^2(m_3 c_{13}^2 + s_{13}^2(m_1 c_{12}^2 + m_2 s_{12}^2)) + d \sin 2\theta_{12} s_{23} c_{23} s_{13} \cos \delta_{CP}] \\
h_{23} &= re^{-i\delta_{CP}}(\eta_{\mu\mu} + \eta_{\tau\tau}) [ds_{12}c_{12}c_{23}^2 s_{13} + s_{23}c_{23}e^{i\delta_{CP}}(m_3 c_{13}^2 + c_{12}^2(m_1 s_{13}^2 - m_2) + s_{12}^2(m_2 s_{13}^2 - m_1)) \\
&\quad - dc_{12}s_{12}s_{13}s_{23}^2 e^{2i\delta_{CP}}] \\
h_{33} &= 2r\eta_{\tau\tau} [s_{23}^2(m_1 s_{12}^2 + m_2 c_{12}^2) + c_{23}^2(m_3 c_{13}^2 + s_{13}^2(m_1 c_{12}^2 + m_2 s_{12}^2)) - d \sin 2\theta_{12} s_{23} c_{23} s_{13} \cos \delta_{CP}]. \quad (13)
\end{aligned}$$

Here $r = \frac{\sqrt{|\Delta m_{31}^2|}}{\Delta m_{31}^2}$ and $d = m_1 - m_2$.

IV. ANALYTICAL EXPRESSIONS FOR ELECTRON NEUTRINO SURVIVAL PROBABILITY

Here we try to derive the formula for $\nu_e \rightarrow \nu_e$ disappearance probability in the presence of scalar NSI. In order to simplify the problem we only consider the diagonal scalar NSI parameters and moreover one NSI parameter at a time while keeping remaining NSI elements to be equal to zero. This way first we present the calculation in the presence of η_{ee} only.

The neutrino evolution equation gets modified in the presence of scalar NSI and is given by in flavour basis as

$$i \frac{\partial}{\partial t} |\nu_f\rangle = H^{\text{eff}} |\nu_f\rangle, \quad (14)$$

where $H^{\text{eff}} = E_\nu + \frac{(M + \delta M)(M + \delta M)^\dagger}{2E_\nu}$.

Neglecting the term proportional to δM^2 Eq. 14 can be rewritten as

$$\begin{aligned} i\frac{\partial}{\partial t}|\nu_f\rangle &= \frac{1}{2E_\nu} \left[U_\nu M_d^2 U_\nu^\dagger + M(\delta M) + (\delta M)M \right] |\nu_f\rangle \\ &= \frac{1}{2E_\nu} \left[U_\nu M_d^2 U_\nu^\dagger + U_\nu D_\nu U_\nu^\dagger (\delta M) + (\delta M) U_\nu D_\nu U_\nu^\dagger \right] |\nu_f\rangle \end{aligned} \quad (15)$$

If we define $U_\nu = U_A U_B$ where $U_A = U_{23} U_\delta$ and $U_B = U_{13} U_\delta^\dagger U_{12}$ then Eq. 15 becomes

$$\begin{aligned} i\frac{\partial}{\partial t}|\nu_f\rangle &= \frac{1}{2E_\nu} \left[U_A U_B M_d^2 U_B^\dagger U_A^\dagger + M(\delta M) + (\delta M)M \right] |\nu_f\rangle \\ &= \frac{1}{2E_\nu} \left[U_A U_B M_d^2 U_B^\dagger U_A^\dagger + U_A U_B D_\nu U_B^\dagger U_A^\dagger (\delta M) + (\delta M) U_A U_B D_\nu U_B^\dagger U_A^\dagger \right] |\nu_f\rangle \end{aligned} \quad (16)$$

Now, if $\delta M \equiv \sqrt{|\Delta m_{31}^2|} \begin{pmatrix} \eta_{ee} & 0 & 0 \\ 0 & 0 & 0 \\ 0 & 0 & 0 \end{pmatrix}$ then it is easy to show that $(\delta M)U_A = U_A(\delta M)$ and using

this fact Eq. 16 can be written in the new basis $|\tilde{\nu}_f\rangle = U_A^\dagger |\nu_f\rangle$ as

$$i\frac{\partial}{\partial t} 2E_\nu |\tilde{\nu}_f\rangle = M^{\text{eff}} |\tilde{\nu}_f\rangle = [M_0 + M_1] |\tilde{\nu}_f\rangle \quad (17)$$

with $M_0 = U_B M_d^2 U_B^\dagger$ and $M_1 = U_B D_\nu U_B^\dagger (\delta M) + (\delta M) U_B D_\nu U_B^\dagger$. The following definitions are to be noted.

$$M_d^2 = \begin{pmatrix} 0 & 0 & 0 \\ 0 & \alpha \Delta m_{31}^2 & 0 \\ 0 & 0 & \Delta m_{31}^2 \end{pmatrix}; D_\nu = \begin{pmatrix} m_1 & 0 & 0 \\ 0 & m_2 & 0 \\ 0 & 0 & m_3 \end{pmatrix}. \quad (18)$$

In the next step we find out the eigenvalues of the M^{eff} and also the modified mixing matrix U'_ν . This is done by first choosing an auxiliary basis $U^{\text{aux}} = U_{13}$ such that $M' = U^{\text{aux}\dagger} M^{\text{eff}} U^{\text{aux}}$:

$$M' = \begin{pmatrix} \alpha s_{12}^2 \Delta m_{31}^2 + \epsilon_2 & \alpha \Delta m_{31}^2 s_{12} c_{12} + s_{12} c_{12} c_{13}^2 \epsilon_3 & s_{31} c_{13} \epsilon_1 \\ \alpha \Delta m_{31}^2 s_{12} c_{12} + s_{12} c_{12} c_{13}^2 \epsilon_3 & \alpha \Delta m_{31}^2 c_{12}^2 & s_{12} c_{12} s_3 c_{13} \epsilon_3 \\ s_{31} c_{13} \epsilon_1 & s_{12} c_{12} s_3 c_{13} \epsilon_3 & \Delta m_{31}^2 + 2m_3 \beta_{ee} s_{13}^2 \end{pmatrix}. \quad (19)$$

Here, $\epsilon_1 = \beta\eta_{ee}(m_1c_{12}^2 + m_2s_{12}^2 + m_3)$, $\epsilon_2 = 2\beta\eta_{ee}c_{13}^2(m_1c_{12}^2 + m_2s_{12}^2)$, and $\epsilon_3 = \beta\eta_{ee}(-m_1 + m_2)$ and $\beta = \sqrt{|\Delta m_{31}^2|}$.

We can express these ϵ 's in terms of the ratios of mass eigenvalues. For NO, we have $\epsilon_1 = \beta\eta_{ee}m_1(c_{12}^2 + \frac{m_2}{m_1}s_{12}^2 + \frac{m_3}{m_1})$, $\epsilon_2 = 2\beta\eta_{ee}c_{13}^2m_1(c_{12}^2 + \frac{m_2}{m_1}s_{12}^2)$, and $\epsilon_3 = \beta\eta_{ee}m_1(-1 + \frac{m_2}{m_1})$. For SI, we have $\frac{m_2}{m_1} \approx 8$ and $\frac{m_3}{m_1} \approx 50$. For IO, we have $\epsilon_1 = \beta\eta_{ee}m_3(\frac{m_1}{m_3}c_{12}^2 + \frac{m_2}{m_3}s_{12}^2 + 1)$, $\epsilon_2 = 2\beta\eta_{ee}c_{13}^2m_3(\frac{m_1}{m_3}c_{12}^2 + \frac{m_2}{m_3}s_{12}^2)$, and $\epsilon_3 = \beta\eta_{ee}m_3(-\frac{m_1}{m_3} + \frac{m_2}{m_3})$. For NO, both $\frac{m_1}{m_3}$ and $\frac{m_2}{m_3} \approx 50$.

We then apply two successive rotations O'_{13} followed by O'_{12} one by one and finally obtain the modified mixing angles by substituting the off diagonal elements of each 2×2 sub-matrix equal to zero after every rotation [65]. We have found that after two rotations H^{eff} is diagonal. The modified mixing angles are given by

$$\tan 2\theta_{13}' = \frac{\sin 2\theta_{13}\epsilon_1}{\Delta m_{31}^2(1 - \alpha s_{12}^2) - \epsilon_2} \quad \text{and} \quad (20)$$

$$\tan 2\theta_{12}' = \frac{-\sin 2\theta_{12}c_{13}(c_{13}\cos\theta\epsilon_3 + \alpha\Delta m_{31}^2c'_{13})}{c_{13}\Delta m_{31}^2(s_{13}'^2 + \alpha s_{12}^2c_{13}'^2) - \alpha\Delta m_{31}^2c_{13}c_{12}^2 + c_{13}'\epsilon_2\cos\theta} \quad (21)$$

where, $\cos\theta = c_{13}c'_{13} - s_{13}s'_{13}$. The corresponding eigenvalues of the effective Hamiltonian M^{eff} are computed as

$$\begin{aligned} \Lambda_1 &= \Delta m_{31}^2(s_{13}'c'_{12})^2 + \alpha\Delta m_{31}^2(c'_{12}c'_{13}s_{12} - c_{12}s'_{12})^2 \\ &\quad + 2\beta\eta_{ee}\cos\theta c'_{12}\left[c'_{12}c_{13}c'_{13}(m_1c_{12}^2 + m_2s_{12}^2) + s_{12}c_{12}c_{13}s'_{12}(m_1 - m_2)\right] \end{aligned} \quad (22)$$

$$\begin{aligned} \Lambda_2 &= \Delta m_{31}^2(s_{12}'s'_{13})^2 + \alpha\Delta m_{31}^2(c_{12}c'_{12} + s_{12}s'_{12}c'_{13})^2 \\ &\quad + 2\beta\eta_{ee}\cos\theta s'_{12}c_{31}\left[s_{12}c_{12}c'_{12}(-m_1 + m_2) + s'_{12}c'_{13}(m_1c_{12}^2 + m_2s_{12}^2)\right] \end{aligned} \quad (23)$$

$$\Lambda_3 = \Delta m_{31}^2c_{13}'^2 + 2\beta\eta_{ee}\sin\theta\left[m_3s_{13}c'_{13} + c_{13}s'_{13}(m_1c_{12}^2 + m_2s_{12}^2)\right], \quad (24)$$

where, $\sin\theta = s_{13}c'_{13} + c_{13}s'_{13}$. Finally, we obtain the PMNS mixing matrix in the presence of scalar

NSI, η_{ee} as

$$\begin{aligned}
U'_\nu &= U_A U^{\text{aux}} O'_{13} O'_{12} \\
&= U_{23}(\theta_{23}) U_\delta U_{13}(\theta_{13}) O'_{13}(\theta'_{13}) O'_{12}(\theta'_{12}) \\
&= U_{23}(\theta_{23}) U_\delta \tilde{U}_{13}(\tilde{\theta}_{13}) O'_{12}(\theta'_{12})
\end{aligned} \tag{25}$$

$$= \begin{pmatrix} c'_{12} \tilde{c}_{13} & s'_{12} \tilde{c}_{13} & \tilde{s}_{13} \\ -c_{23} s'_{12} - c'_{12} \tilde{s}_{13} s_{23} e^{i\delta} & c_{23} c'_{12} - s'_{12} \tilde{s}_{13} s_{23} e^{i\delta} & \tilde{c}_{13} s_{23} e^{i\delta} \\ s_{23} s'_{12} - c'_{12} \tilde{s}_{13} c_{23} e^{i\delta} & -s_{23} c'_{12} - s'_{12} \tilde{s}_{13} c_{23} e^{i\delta} & \tilde{c}_{13} c_{23} e^{i\delta} \end{pmatrix} \tag{26}$$

where, $\tilde{s}_{13} = \sin \tilde{\theta}_{13}$ and $\tilde{\theta}_{13} = \theta_{13} + \theta'_{13}$. Thus, scalar NSI modified mixing matrix is easy to obtain from the vacuum mixing matrix by just replacing the following parameters from the vacuum one:

$$\begin{aligned}
\theta'_{23} &= \theta_{23} \\
\delta' &= \delta \\
\theta_{13} &\rightarrow \tilde{\theta}_{13} \\
\theta_{12} &\rightarrow \theta'_{12}.
\end{aligned} \tag{27}$$

The electron antineutrino survival probability in vacuum is given by [66]

$$\begin{aligned}
P_{ee} &= 1 - \cos^4 \theta_{13} \sin^2 2\theta_{12} \sin^2 \Delta_{21} \\
&\quad - \sin^2 2\theta_{13} \sin^2 (|\Delta_{31}|) \\
&\quad - \sin^2 \theta_{12} \sin^2 2\theta_{13} \sin^2 \Delta_{21} \cos (2|\Delta_{31}|) \\
&\quad \pm \frac{\sin^2 \theta_{12}}{2} \sin^2 2\theta_{13} \sin (2\Delta_{31}) \sin (2|\Delta_{31}|).
\end{aligned} \tag{28}$$

In the above equation, only the last term is sensitive to the mass ordering where plus sign corresponds to NO and minus corresponds to IO. We also note that the dependence on θ_{13} -terms is only via $\sin^2 2\theta_{13}$ and therefore is a second-order effect. We calculate the value of P_{ee} analytically in the presence of η_{ee} by substituting the eigenvalues from vacuum to the mass eigenvalues obtained in Eqs. 22, 23, 24 and mixing angles as given in Eq. 27 in Eq. 28. The results match very well with the numerically-obtained exact probability values for all oscillation channels.

From Eq. 20, we note that the η_{ee} -correction to θ_{13} is itself θ_{13} -suppressed. Thus, we expect θ_{13} measurements to not be affected by η_{ee} . Further, since in Eq. 28, θ_{13} -terms are second-order, we do not expect any significant effect of η_{ee} on P_{ee} through θ'_{13} . In order to gauge the effect of η_{ee} on the dominant θ_{12} term, we approximate $\theta'_{13} \approx 0$.

We then have,

$$\tan 2\theta_{12}' = \frac{\sin 2\theta_{12} (\Delta m_{21}^2 + \epsilon_3 \cos^2 \theta_{13})}{\Delta m_{21}^2 \cos 2\theta_{12} - \epsilon_2}. \quad (29)$$

Therefore, for $\epsilon_2, \epsilon_3 \ll \Delta m_{21}^2$, we do not expect any significant modification in θ_{12} because of η_{ee} . Similarly, for the mass-squared differences we get

$$\begin{aligned} \Delta m_{21}^{2'} &= \Lambda_2 - \Lambda_1 \\ &= \Delta m_{21}^2 \cos 2(\theta_{12} - \theta_{12}') + \cos^2 \theta_{13} \sin 2\theta_{12} \sin 2\theta_{12}' \epsilon_3 - \cos 2\theta_{12}' \epsilon_2 \end{aligned} \quad (30)$$

$$(31)$$

The η_{ee} -correction to Λ_3 is also suppressed by $\sin \theta_{13}$. On substituting $\theta_{13}' = 0$, we get $\Lambda_3 = \Delta m_{31}^2 + 2\beta\eta_{ee}m_3 \sin^2 \theta_{13}$. Hence, we approximate $\Lambda \approx \Delta m_{31}^2$. So η_{ee} -modified atmospheric mass-squared difference is

$$\begin{aligned} \Delta m_{31}^{2'} &= \Lambda_3 - \Lambda_1 \\ &= \Delta m_{31}^2 - \Delta m_{21}^2 \sin^2 (\theta_{12} - \theta_{12}') \\ &\quad - \cos^2 \theta_{12}' \epsilon_2 - \frac{1}{2} \cos^2 \theta_{13} \sin 2\theta_{12} \sin 2\theta_{12}' \epsilon_3 \end{aligned} \quad (32)$$

The computation for the electron neutrino survival probability when scalar NSI parameter $\eta_{\mu\mu}$ or $\eta_{\tau\tau}$ is present has been performed in Appendix A. *Here, it is worthwhile to mention that the probability P_{ee} becomes dependent on θ_{23} and δ_{CP} in the presence of $\eta_{\mu\mu}$ or/and $\eta_{\tau\tau}$ even in the vacuum which is not the case in the standard three flavour oscillation picture.*

V. OSCILLATION PROBABILITY IN THE PRESENCE OF SCALAR NSI

In Fig. 1, we show the effect of scalar NSI on the electron antineutrino survival probability $P(\bar{\nu}_e \rightarrow \bar{\nu}_e) = P_{ee}$ plotted as a function of the antineutrino energy for JUNO baselines corresponding to $L = 53$ km. The value of the standard neutrino oscillation parameters have been taken from table I except θ_{23} and δ_{CP} which are taken to be 45° and 0° respectively. The left panel corresponds to choice of NMO being NO while the right panel corresponds to it being IO. We consider only one diagonal scalar NSI $\eta_{\alpha\alpha}$ ($\alpha = e, \mu, \tau$) to be non-zero at a time. The top, middle and bottom panels in Fig. 1 show the variation in P_{ee} with η_{ee} , $\eta_{\mu\mu}$ and $\eta_{\tau\tau}$ respectively.

Oscillation parameters (3ν)	Normal ordering	Inverse Ordering
θ_{12}°	$33.41^{+0.75}_{-0.72}$	$33.41^{+0.75}_{-0.72}$
θ_{23}°	$42.2^{+1.1}_{-0.9}$	$49.0^{+1.0}_{-1.2}$
θ_{13}°	$8.58^{+0.11}_{-0.11}$	$8.57^{+0.11}_{-0.11}$
δ_{CP}°	232^{+36}_{-26}	276^{+22}_{-29}
Δm_{21}^2 (eV ²)	$7.41^{+0.21}_{-0.20} \times 10^{-5}$	$7.41^{+0.21}_{-0.20} \times 10^{-5}$
Δm_{3l}^2 (eV ²)	$+2.507^{+0.026}_{-0.027} \times 10^{-3}$	$-2.486^{+0.025}_{-0.028} \times 10^{-3}$

TABLE I: Best-fit values of the neutrino oscillation parameters considering the standard three-flavor scenario. These values with 1σ interval are taken from NuFIT 5.2 (2022), including Super-K atmospheric data [5]

We have used GLOBES [67, 68] to generate the oscillation probabilities by appropriately modifying the inbuilt probability functions to incorporate scalar NSI in vacuum. As mentioned before, our numerical calculations for probabilities match very well with the analytical expressions derived in Sec. IV and also with other works on scalar NSI (sNSI) [44, 63].

For NO, we vary $\eta_{\alpha\alpha}$ ($\alpha = e, \mu, \tau$) in the range $[-0.04, 0.04]$ and for IO we vary them in the range $[-0.008, 0.008]$. As we will see, the magnitude of these ranges correspond to the value of scalar NSI that give non-negligible deviations in P_{ee} from the standard, three-flavor framework expectation (SI). The solid black curve in each plot of Fig. 1 corresponds to SI. Probabilities corresponding to the positive (negative) values of sNSI parameter in each plot are shown with solid (dashed) curves. From Fig. 1, we make the following observations.

- We observe two discernible oscillatory features in P_{ee} for the given choice of energies and baseline. The longer-wavelength oscillations are Δm_{21}^2 -driven while the smaller-wavelength oscillations are Δm_{31}^2 -driven. As argued in Sec. IV, the effect of sNSI on θ_{13} is small. If we only look at the change in the Δm_{21}^2 -driven oscillations, we see that in each plot there is an energy at which the positive and negative η probabilities coincide. For example, in the case of η_{ee} and NO, this occurs at $E_{\bar{\nu}} \approx 2$ MeV while for $\eta_{\mu\mu}$ and NO, this occurs at $E_{\bar{\nu}} \approx 3$ MeV. The enhancing or suppression of P_{ee} , compared to the standard case, as a function of the sign of $\eta_{\alpha\alpha}$ flips at this energy value.
- The effect of positive (negative) η_{ee} is to suppress (enhance) P_{ee} compared to the SI case. This behaviour of η_{ee} is observed for both NO and IO and can be seen in the top panels of

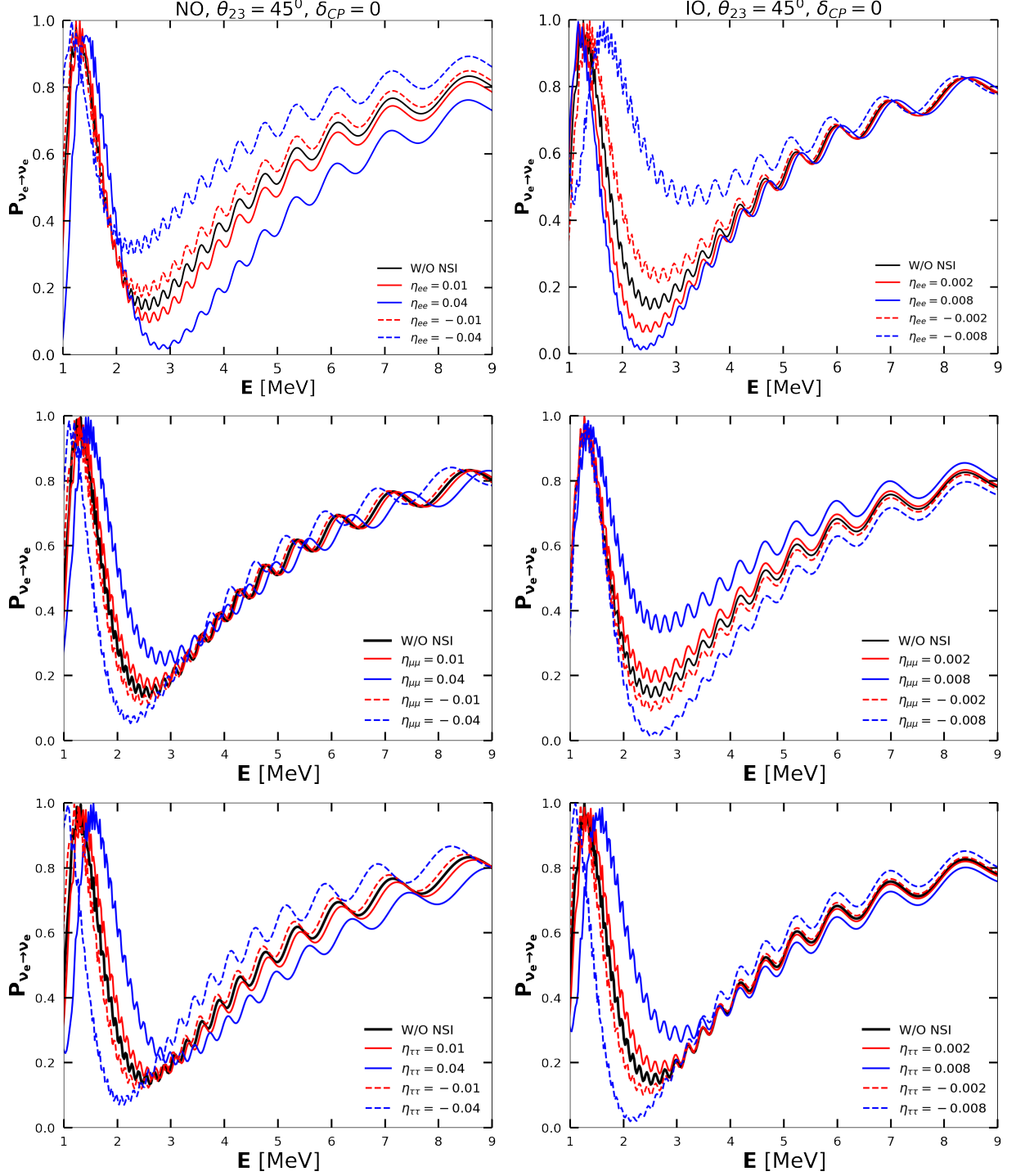


FIG. 1: $P(\bar{\nu}_e \rightarrow \bar{\nu}_e)$ as a function of antineutrino energy for JUNO ($L = 53$ km). The left(right) panel is for NO(IO). The top, bottom and middle panels are for η_{ee} , $\eta_{\mu\mu}$ and $\eta_{\tau\tau}$ respectively. The probabilities for the standard case (marked SI) are shown in black.

Fig. 1.

- For $\eta_{\mu\mu}$ and NO (see middle left plot of Fig. 1) P_{ee} increases with positive $\eta_{\mu\mu}$ in the energy range ~ 1.8 MeV to 3.0 MeV and decreases after that. The negative $\eta_{\mu\mu}$ has the opposite behaviour. For IO (middle right plot of Fig. 1) positive and negative $\eta_{\mu\mu}$ P_{ee} coincide at around 1.2 MeV. As a result, the positive (negative) $\eta_{\mu\mu}$ enhances (suppresses) P_{ee} for the JUNO-relevant energy range of 2 – 8 MeV.
- For $\eta_{\tau\tau}$, P_{ee} is enhanced for the positive values of $\eta_{\tau\tau}$ in the energy range ~ 1.8 MeV to 3.0 MeV (see lower panels of Fig. 1) and is suppressed in energy range beyond ~ 3.0 MeV. The behavior of P_{ee} with negative values of $\eta_{\tau\tau}$ is opposite to that with positive values of $\eta_{\tau\tau}$. We observe this for both NO and IO.
- An important feature to be noticed is that significant deviations are observed in P_{ee} in the case IO with sNSI values an order of magnitude lower compared to what we observe for NO. Thus, we expect JUNO to impose stronger constraints on diagonal sNSI for IO.

VI. THE JUNO EXPERIMENT

The Jiangmen Underground Neutrino Observatory (JUNO) experiment [69] is a multi-national neutrino experiment based in China. It is in the construction phase currently and is scheduled to start taking data as early as 2024. It aims to observe reactor antineutrinos from several nuclear power plants located at Yangjiang and Taishan. It will consist of a 20 kton fiducial mass liquid scintillator detector situated at an average baseline of approximately 53 km from the reactors. This detector is projected with the ability to reconstruct the incoming neutrino energy with an unprecedented $[\Delta E/E \sim 0.03/\sqrt{E_{\text{vis}}(\text{MeV})}]$ [69].

The main goal of JUNO is to measure the NMO. In addition, it will also be able to measure θ_{12} , Δm_{21}^2 and Δm_{31}^2 quite precisely. The distant reactors at Daya Bay and Huizhou will also have small contributions at JUNO but in this work we ignore these reactor cores. In this work, we have considered the various reactor cores (with their respective thermal powers and baselines) at the Yangjiang and Taishan nuclear power plants as mentioned in Table 2 of [69]. The details of backgrounds and systematical errors is same as in [69]. For the analysis presented in this work, we consider a combined signal and background events of around 140,000. The signal at JUNO is the inverse beta-decay (IBD) events $\bar{\nu}_e + p \rightarrow e^+ + n$. The bulk of the signal will lie in the energy range $\sim [1.8, 8]$ MeV. The antineutrino fluxes and IBD cross-sections are relatively well-known [69].

We have simulated the JUNO experiment¹ using GLoBES [67, 68]. We have also used this software package to generate events plots and the sensitivity results described in Sec. VII and Sec. VIII.

VII. EVENT RATES WITH JUNO IN THE PRESENCE OF SCALAR NSI

In this section we present the simulated event rates at JUNO in presence of sNSI and discuss some important features of the event spectra congruent with those observed in the probability plots in Fig. 1. We consider reconstructed antineutrino energy in the range (1.8, 8.0) MeV divided into 200 bins of 0.031 MeV bin-width. We show results only for the diagonal sNSI $\eta_{\alpha\alpha}$ ($\alpha = e, \mu, \tau$). We assume these to be real and set the remaining off-diagonal sNSI to be 0. We choose the mass of the lightest mass eigenstate to be 10^{-3} eV. For NO, the lightest mass eigenstate is m_1 while for IO it is m_3 . The value of standard oscillation parameters are taken from Table I.

The results are shown in Figs. 2 for NO and 3 for IO. The left (right) panels in these figures correspond to positive (negative) values of the sNSI parameters. The standard events rates are shown in red. In the top panel of Fig. 2, we consider $|\eta_{\alpha\alpha}| = 0.012$. As we will see later, this value of η roughly corresponds to the upper 3σ -allowed limit of the sNSI constraints with JUNO for NO. In the bottom panel of Fig. 2, we show the relative difference in the number of expected events per neutrino energy bin for two sets of positive and negative sNSI parameters. These sNSI values correspond to slightly larger and slightly smaller choices compared to the top panel. Fig. 3 is generated in a similar way, but for IO. Note that in case of Fig. 3 we choose $|\eta_{\alpha\alpha}|$ such that they correspond to the 3σ -allowed upper limit for IO. From Figs. 2 and 3 the following observations can be made.

- It can be observed from the upper panels of Fig. 2 that inclusion of positive (negative) values of $\eta_{\mu\mu}$ and $\eta_{\tau\tau}$ enhances (suppresses) the event rates by almost 10 -15 % (vide lower left (right) panels of Fig. 2) in the lower energy range ~ 2.2 - 3.5 MeV. Beyond ~ 3.5 MeV deviation in rates due to $\eta_{\mu\mu}$ and $\eta_{\tau\tau}$ are diminished. However, positive (negative) η_{ee} is to suppress (enhance) event rates for the neutrino energy range of ~ 2.5 MeV to 6.0 MeV. This indicates that $\eta_{\mu\mu}$ and $\eta_{\tau\tau}$ influence the oscillation (and hence the event rates) due to the effects of solar Δm_{21}^2 and θ_{12} more in the lower energy range of ~ 2.2 to 3.5 MeV while the

¹ Our simulation of JUNO is much-simpler than a detailed one that the experimental collaboration uses. However, it suffices our aim of making a phenomenological prediction of JUNO's ability to constrain/discover new physics.

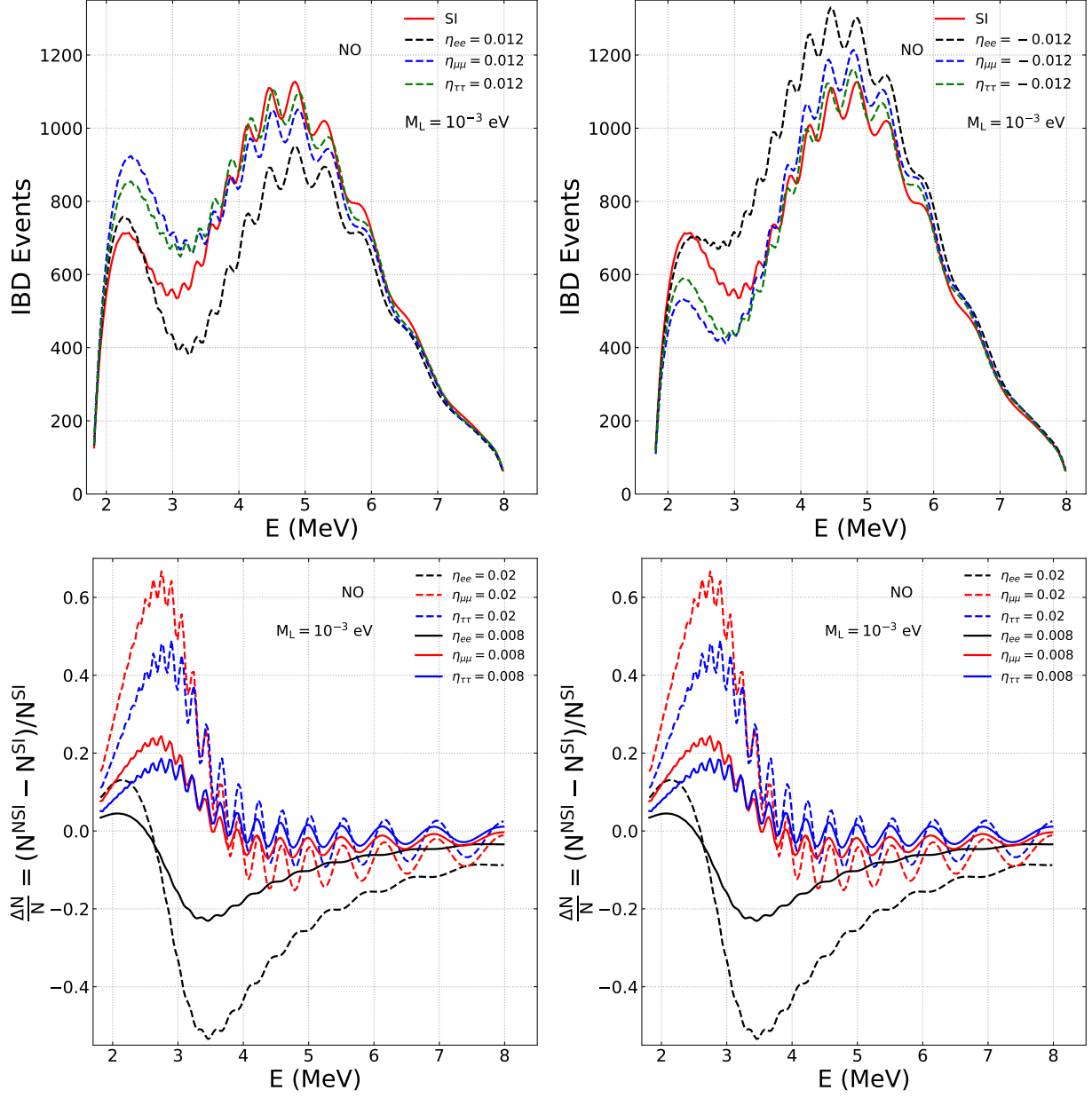


FIG. 2: Event rates at JUNO assuming NO in the presence of sNSI. The top panel shows the events rates for the standard case, and for $|\eta_{\alpha\alpha}$ ($\alpha = e, \mu, \tau$) = 0.012. The bottom panel shows the relative change in event rates with sNSI compared to the standard case for $|\eta_{\alpha\alpha}$ ($\alpha = e, \mu, \tau$) = 0.008, 0.02. The left (right) panel is for positive (negative) η .

NSI parameter η_{ee} affects the oscillations in a larger neutrino energy range of ~ 2.2 to 6.0 MeV. Thus, we expect the effects of η_{ee} to be present in statistically-larger event samples.

- On comparing the upper panels of Figs. 2 and 3 we notice that the effects of sNSI are more pronounced for IO since even with smaller values of NSI parameters (say for instance, $|\eta_{\alpha\alpha}| =$

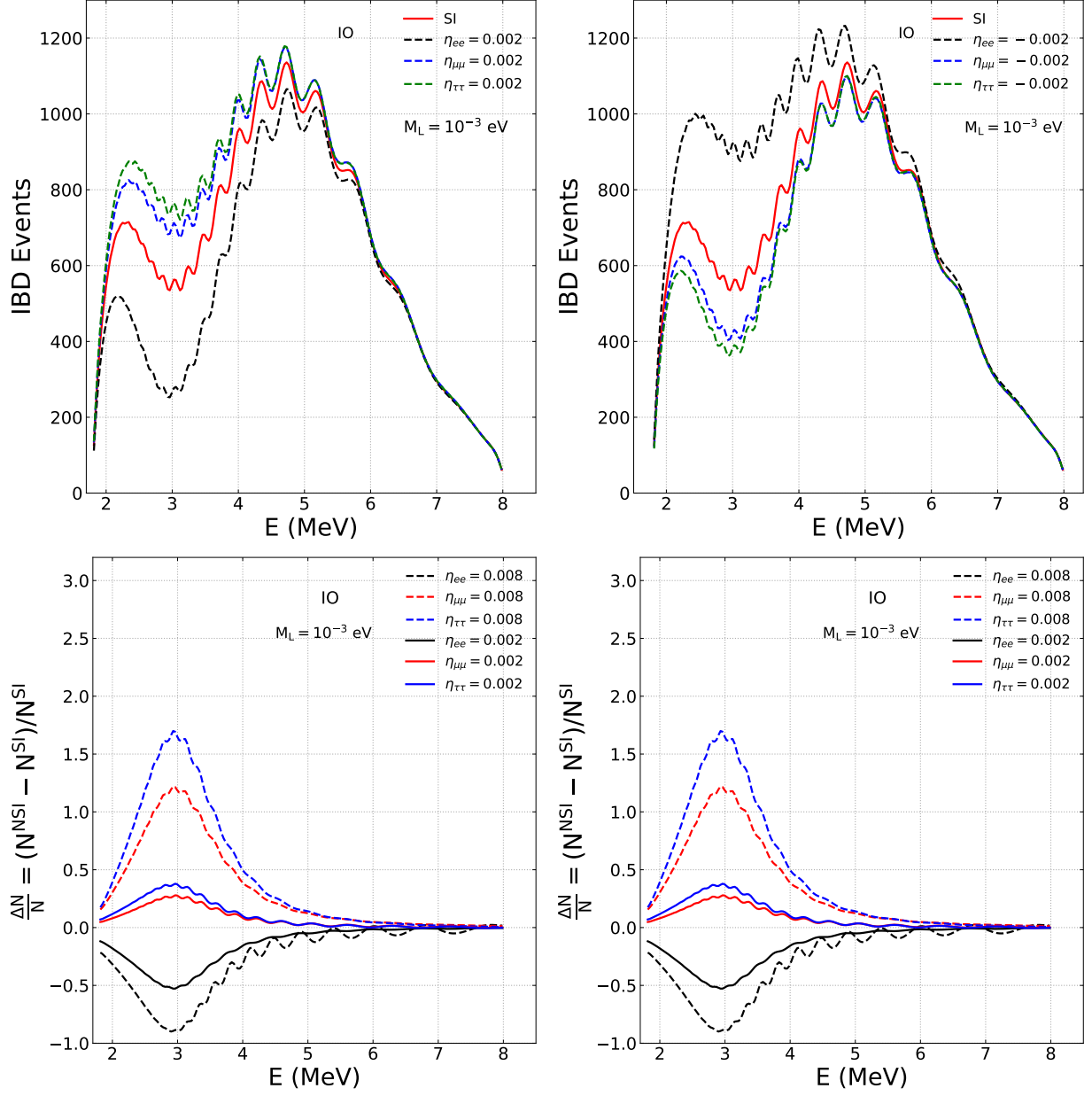


FIG. 3: Same as in Fig. 3 but for IO.

0.002 which is one order magnitude smaller than the NO case) significant modifications are observed in the event rates.

- For the IO case the spectra are less degenerate with the standard case. This should again assist in better exclusion of sNSI for IO.

VIII. RESULTS

In this section, we estimate the sensitivity of JUNO towards neutrino oscillation measurements in the presence of sNSI. As discussed before, these results correspond to a total exposure such that a total of around 140,000 signal and background events are observed.

We show results at the 3σ confidence level for both NO and IO, positive and negative values of diagonal sNSI keeping only one η active at a time. Next, we elucidate the numerical procedure for calculating the χ^2 . We simulate the data or the “true” observed event rates assuming some true values of the neutrino oscillation parameters. We always assume the standard case where there is no sNSI present. Next, we test this data against the theoretical (or “fit”) event rates i.e. the simulated events calculated assuming the existence of sNSI in the theoretical framework.

In GLoBES, the formula for the total χ^2 is given as follows:

$$\begin{aligned} \chi_{\text{total}}^2 = & \sum_{i=1}^n 2 [F_i (1 + \xi_1 + \xi_2) - D_i + D_i \ln (D_i / F_i (1 + \xi_1 + \xi_2))] \\ & + \sum_k (\xi_k / \sigma_k)^2 + \sum_j (\theta_j - \theta_j^{\text{bf}})^2 / \sigma_j^2. \end{aligned} \quad (33)$$

Here $n = 200$ is the total number of reconstructed energy bins for JUNO. F_i is the fit events and D_i is the true events for a given energy bin. ξ_k and σ_k represent the systematic errors and standard deviation in the errors respectively. j represents the number of oscillation parameters that are varied in the fit. θ_j^{bf} to the central value oscillation parameters θ_j , and σ_j is the 1σ uncertainty in them. We consider a combined normalisation error of $\xi_1 = 5\%$ (20%) for signal (background) events and an energy calibration error of $\xi_2 = 3\%$. In order to take into account the present uncertainty in the knowledge of a given oscillation parameter, we calculate the χ_{total}^2 for each value in the $(-3\sigma, +3\sigma)$ range. The smallest χ_{total}^2 in this range is selected and is reported as the least- χ^2 . We show the allowed regions corresponding to $\Delta\chi^2 = 11.83$ for 2 degree of freedom (DOF) for different cases.

A. Constraints on scalar NSI

We first present the results for JUNO’s potential to constrain sNSI. The results are shown in the $m_{\text{lightest}} - |\eta_{\alpha\alpha}|$ parameter space in Fig. 4. In each case, we show the results for both NO and IO and for both positive and negative values of η . We assume the true to be the standard case when all $\eta_{\alpha\alpha} = 0$. In the test, we vary m_{lightest} and $\eta_{\alpha\alpha}$ in the range as shown in the plots. We marginalise over θ_{12} , Δm_{21}^2 and Δm_{31}^2 in the allowed $\pm 3\sigma$ range. For every $(m_{\text{lightest}}, |\eta_{\alpha\alpha}|)$, we

obtain a least- χ^2 between the true and fit. We find that the results for both positive and negative values of sNSI parameters are very similar and overlap closely with each other. In all the three cases, the results for IO are better than NO in each case by almost an order of magnitude.

We find that in the case of NO, for $m_1 \lesssim 10^{-2}$ eV, $|\eta_{ee}|, |\eta_{\mu\mu}|, |\eta_{\tau\tau}| \lesssim 10^{-2}$ is allowed at 3σ . If $m_1 \approx 10^{-1}$ eV then $|\eta_{ee}|, |\eta_{\mu\mu}|, |\eta_{\tau\tau}| \lesssim 10^{-3}$ is allowed at 3σ . For IO, if $m_1 \lesssim 10^{-2}$ eV, $|\eta_{ee}|, |\eta_{\mu\mu}|, |\eta_{\tau\tau}| \lesssim (1-2) \times 10^{-3}$ is allowed at 3σ .

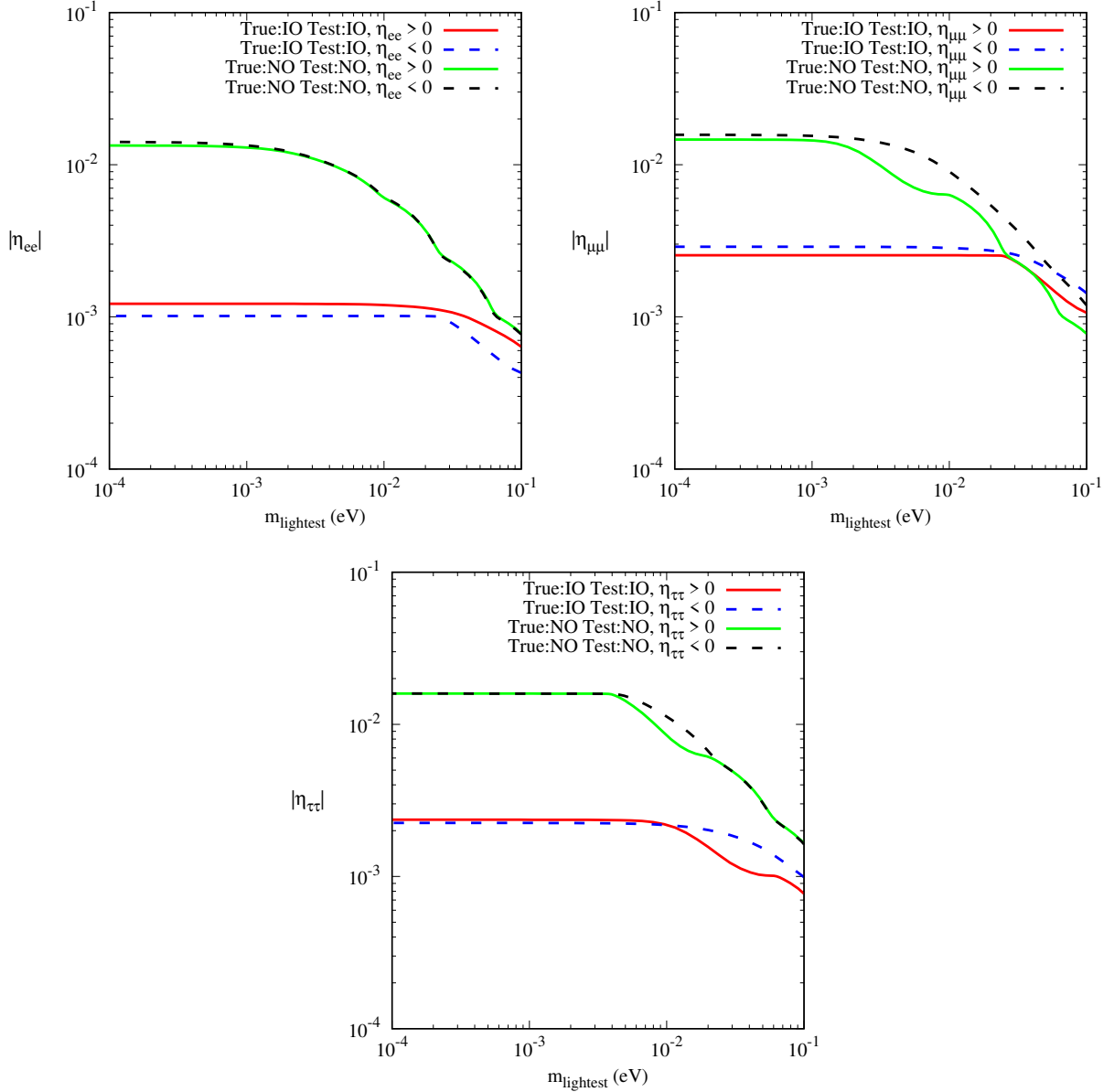


FIG. 4: Constraints on sNSI with JUNO. Top left (right) panel is for $|\eta_{ee}|$ ($|\eta_{\mu\mu}|$). Bottom panel is for $|\eta_{\tau\tau}|$.

B. Mass ordering sensitivity in the presence of scalar NSI

We next show the results for exclusion of the wrong mass-ordering with JUNO in Fig. 5. The computation exercise is exactly same as that for Fig. 4 except the important difference that in the fit, the mass ordering is opposite to what has been assumed in the true. We find that the results for the positive and negative $\eta_{\alpha\alpha}$ are almost exactly degenerate in all the three cases. Our results show that the wrong hierarchy is allowed at 3σ depending on the values of m_{lightest} and $|\eta_{\alpha\alpha}|$. For example, if IO is the true hierarchy, then NO is allowed if $|\eta_{ee}| \lesssim 5 \times 10^{-2}$ and test $m_3 \lesssim 10^{-3}$ eV. Similar conclusions can be drawn for the other mass ordering and $\eta_{\alpha\alpha}$.

C. Precision measurements in the presence of scalar NSI

We now analyse the ability of JUNO to precisely measure the neutrino oscillation parameters if sNSI is present in nature. We generate the true or observed event spectrum assuming standard interactions and the value of oscillation parameters as given in Table I. In the fit, we first assume the standard case and calculate the precision of the standard oscillation parameters namely $\sin^2 \theta_{12}$, Δm_{21}^2 , and Δm_{31}^2 . The results are shown as the black line in Figs. 6, 7 and 8. Note that in each case, we marginalise over the relevant parameters. We next switch on one diagonal sNSI at a time and for each value of the test oscillation parameter in Figs. 6, 7 and 8 i.e. $\sin^2 \theta_{12}$, Δm_{21}^2 , and Δm_{31}^2 , we marginalise over the $\pm 3\sigma$ -allowed range as calculated in Fig. 4. The results are shown as orange, blue and red line corresponding to marginalisation over η_{ee} , $\eta_{\mu\mu}$ and $\eta_{\tau\tau}$, respectively, in the fit.

We find that depending on the NMO and the oscillation parameter, there is worsening in the precision measurement to different extent. We tabulate our results in Table II to show the $\pm 1\sigma$ uncertainty in the measurement of oscillation parameters in the standard case and in the presence of sNSI.

IX. SUMMARY AND CONCLUDING REMARKS

In this work, we explore the impact of scalar non-standard interactions (sNSI) on neutrino oscillation measurements at JUNO. We derive the expressions for electron antineutrino survival probability considering only the diagonal sNSI elements - taking only one to be non-zero at a

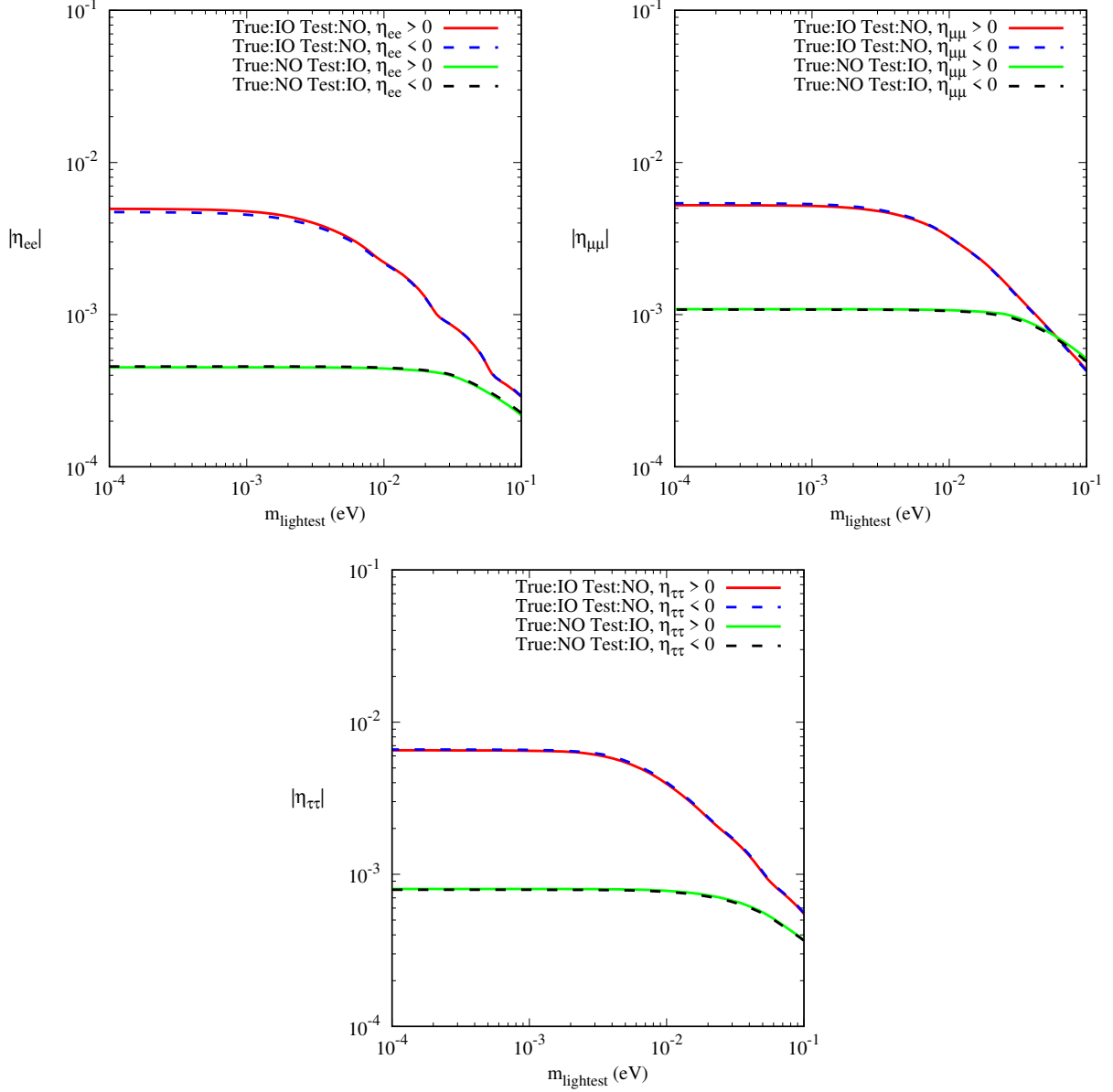


FIG. 5: Wrong mass-ordering exclusion with JUNO in the presence of sNSI. Top left (right) panel is for $|\eta_{ee}|$ ($|\eta_{\mu\mu}|$). Bottom panel is for $|\eta_{\tau\tau}|$.

time. For the case of η_{ee} , we calculate the full probability expression using the rotation technique whereas a semi-analytical approach is exercised for $\eta_{\mu\mu}$ (or $\eta_{\tau\tau}$) which is presented in Appendix A. We do not consider the standard Earth matter effects which is a good assumption for JUNO baselines (≈ 53 km) and antineutrino energies ($\approx 1 - 8$ MeV). We demonstrate the results for both normal and inverted neutrino mass ordering and also consider positive as well as negative values of the sNSI parameters.

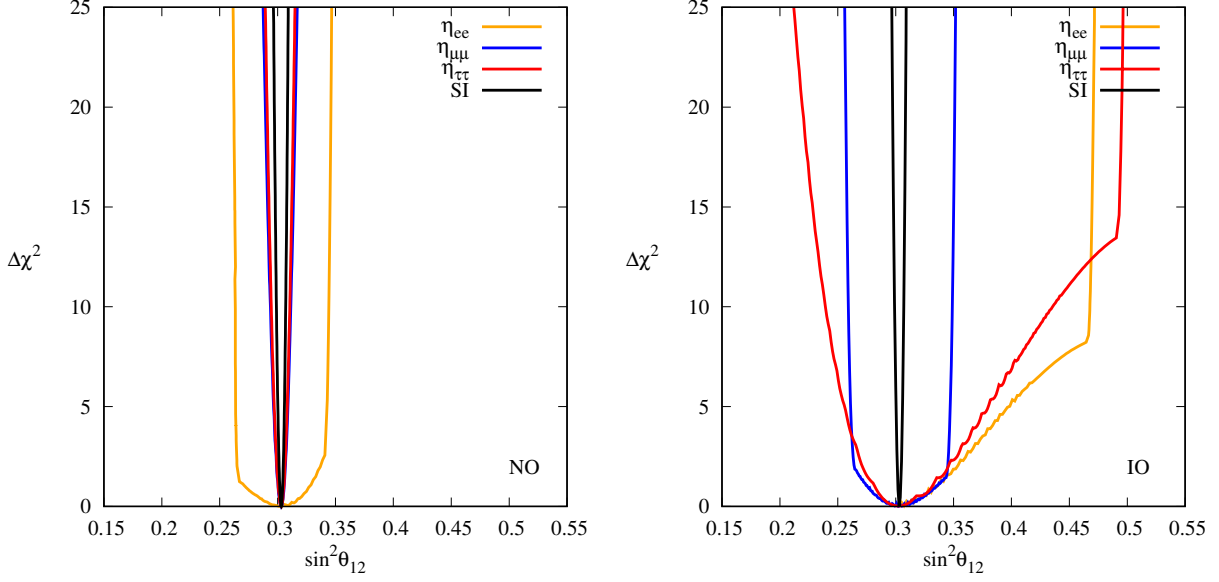


FIG. 6: Precision measurement of $\sin^2 \theta_{12}$ in the presence of sNSI. Left (right) panel is for NO (IO).

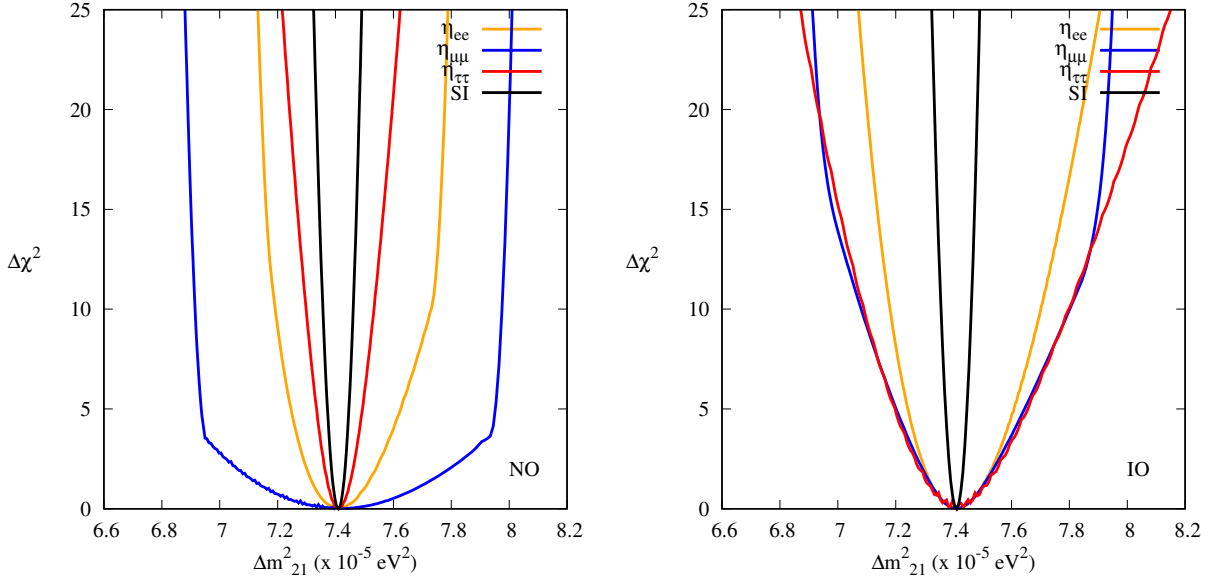


FIG. 7: Precision measurement of Δm_{21}^2 in the presence of sNSI. Left (right) panel is for NO (IO).

sNSI appear as corrections to the neutrino masses in the Hamiltonian. These corrections are independent of neutrino energies and appear as product of $\sqrt{|\Delta m_{31}^2|}$, $\eta_{\alpha\alpha}$ and m_{lightest} . For a given NMO, $\sqrt{|\Delta m_{31}^2|}$ is more or less known now. Thus, the results are shown as correlated functions of $\eta_{\alpha\alpha}$ and m_{lightest} . We find that JUNO can provide the most stringent constraints on the diagonal sNSI. For NO, depending on the value of m_1 , JUNO can exclude $|\eta_{ee}|, |\eta_{\mu\mu}|, |\eta_{\tau\tau}| \gtrsim 10^{-3}$ to 10^{-2}

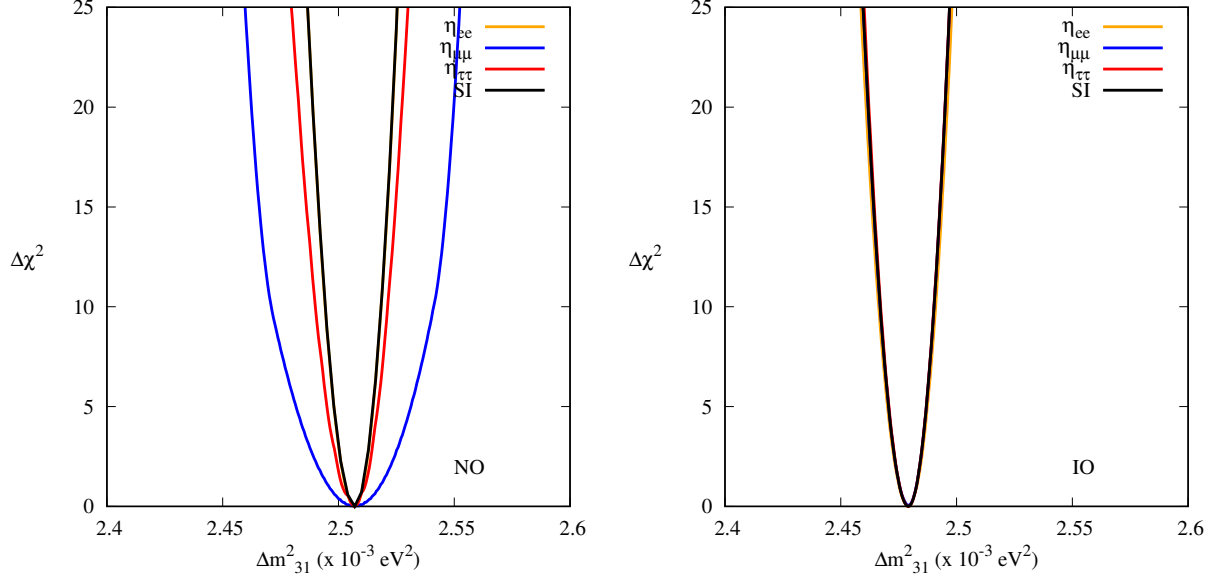


FIG. 8: Precision measurement of Δm_{31}^2 in the presence of sNSI. Left (right) panel is for NO (IO).

Parameters (3ν)	NMO	SI (%)	η_{ee} (%)	$\eta_{\mu\mu}$ (%)	$\eta_{\tau\tau}$ (%)
$\sin^2 \theta_{12}$	NO	0.13	0.9	0.3	0.26
$\sin^2 \theta_{12}$	IO	0.13	2.7	0.96	2.8
Δm_{21}^2	NO	1.6	6.6	11.3	4.1
Δm_{21}^2	IO	1.7	8.3	10.4	12.8
Δm_{31}^2	NO	0.39	0.39	0.93	0.50
Δm_{31}^2	IO	0.37	0.39	0.37	0.37

TABLE II: 1σ uncertainty in the precision measurements of neutrino oscillation parameters with JUNO in the presence of sNSI.

at 3σ C.L. For IO, the exclusion reach is better and the constraints an-order-of-magnitude smaller can be obtained for the same value of m_3 . sNSI can also diminish the NMO exclusion sensitivity of JUNO, although only at the 3σ C.L. In Fig. 5, we show that for a given true value of NMO, the wrong mass ordering is allowed at 3σ for certain allowed values of sNSI parameters in the $\eta_{\alpha\alpha}$ - m_{lightest} parameter space. Finally in Table II, we show the impact in precision measurement of $\sin^2 \theta_{12}$, Δm_{21}^2 and Δm_{31}^2 . We find that JUNO can measure these parameters to about 0.6% or better for the standard case. sNSI, however, can worsen the precision measurement to as high as 13%.

Appendix A: Analytical expression in the case of $\eta_{\mu\mu}$

If we switch on the $\eta_{\mu\mu}$ as the only source of scalar NSI then above rotation technique is not working due to the presence of complex CP phase δ_{CP} in the effective Hamiltonian H^{eff} . So, in this case we apply the Faddeev-LeVerrier algorithm as described in [70] to get the semi-analytical expression for P_{ee} . According to this method first, we write down the Hamiltonian in vacuum mass basis (H^{vac}) and then devise the characteristic equation given as

$$\lambda^3 + B_0\lambda^2 + B_1\lambda + K = 0 \quad (\text{A1})$$

where

$$B_0 \equiv -\text{Tr}H^{\text{vac}}, \quad B_1 \equiv \frac{1}{2}(B_0^2 - \text{Tr}(H^{\text{vac}})^2), \quad K \equiv -\det H^{\text{vac}}. \quad (\text{A2})$$

From Eq. 15 one can easily write down the Hamiltonian in mass basis in vacuum as

$$H^{\text{vac}} = \frac{M_d^2}{2E_\nu} + \frac{1}{2E_\nu} \left(D_\nu U_\nu^\dagger (\delta M) U_\nu + U^\dagger (\delta M) U_\nu D_\nu \right) \quad (\text{A3})$$

We write the matrix elements of the Hamiltonian H^{vac} as

$$H_{11}^{\text{vac}} = m_1^2 + 2m_1\beta\eta_{\mu\mu}c_{23}s_{12}(c_{23}s_{12} + 2c_{12}s_{13}s_{23}\cos\delta_{\text{CP}}), \quad (\text{A4a})$$

$$H_{12}^{\text{vac}} = (m_1 + m_2)\beta\eta_{\mu\mu} \left[s_{12}c_{12}(s_{13}^2s_{23}^2 - c_{23}) + (e^{i\delta_{\text{CP}}}s_{12}^2 - e^{-i\delta_{\text{CP}}}c_{12}^2)s_{13}s_{23}c_{23} \right], \quad (\text{A4b})$$

$$H_{13}^{\text{vac}} = -(m_1 + m_3)\beta\eta_{\mu\mu}c_{13}s_{23}(c_{23}s_{12} + c_{12}s_{13}s_{23}e^{-i\delta_{\text{CP}}}), \quad (\text{A4c})$$

$$H_{22}^{\text{vac}} = m_2^2 + 2m_2\beta\eta_{\mu\mu}c_{12}c_{23}(c_{12}c_{23} - 2s_{12}s_{23}s_{13}\cos\delta_{\text{CP}}), \quad (\text{A4d})$$

$$H_{23}^{\text{vac}} = (m_2 + m_3)\beta\eta_{\mu\mu}c_{13}s_{23}(c_{12}c_{23} - e^{-i\delta_{\text{CP}}}s_{12}s_{13}s_{23}), \quad (\text{A4e})$$

$$H_{33}^{\text{vac}} = m_3^2 + 2\beta\eta_{\mu\mu}m_3c_{13}^2s_{23}^2. \quad (\text{A4f})$$

From Eqs. A2 and A4a to A4f we have

$$B_0 = -(m_1^2 + m_2^2 + m_3^2) - 2\beta\eta_{\mu\mu} \left[c_{23}^2(m_1s_{12}^2 + m_2c_{12}^2) + m_3s_{23}^2c_{13}^2 + (m_1 - m_2)\sin 2\theta_{12}s_{23}c_{23}s_{13}\cos\delta_{\text{CP}} \right], \quad (\text{A5})$$

$$B_1 = (m_1m_2)^2 + (m_2m_3)^2 + (m_3m_1)^2 + 2\beta\eta_{\mu\mu} \left[c_{23}^2(m_1m_2\chi^{1c} + m_3^2\chi^{1s}) + c_{13}^2s_{23}^2m_3(m_1^2 + m_2^2) - \frac{1}{2}\sin 2\theta_{12}\sin 2\theta_{23}s_{13}\cos\delta_{\text{CP}}(m_1 - m_2)(m_1m_2 - m_3^2) \right], \quad (\text{A6})$$

$$K = (m_1m_2m_3)^2 + 2m_1m_2m_3\beta\eta_{\mu\mu} \left[m_3c_{23}^2\chi^{1c} + m_1m_2c_{13}^2s_{23}^2 - \frac{1}{2}\sin 2\theta_{12}\sin 2\theta_{23}s_{13}(m_1 - m_2)m_3\cos\delta_{\text{CP}} \right], \quad (\text{A7})$$

where we have defined

$$\chi^{1c} = m_1 c_{12}^2 + m_2 s_{12}^2 \quad (\text{A8a})$$

$$\chi^{1s} = m_1 s_{12}^2 + m_2 c_{12}^2 \quad (\text{A8b})$$

The eigenvalues of the H^{vac} are given by

$$\lambda_1 = \frac{1}{3}B_0 - \frac{1}{3}\sqrt{B_0^2 - 3B_1} \cos \gamma - \frac{1}{\sqrt{3}}\sqrt{B_0^2 - 3B_1} \sin \gamma \quad (\text{A9})$$

$$\lambda_2 = \frac{1}{3}B_0 - \frac{1}{3}\sqrt{B_0^2 - 3B_1} \cos \gamma + \frac{1}{\sqrt{3}}\sqrt{B_0^2 - 3B_1} \sin \gamma \quad (\text{A10})$$

$$\lambda_3 = \frac{1}{3}B_0 + \frac{2}{3}\sqrt{B_0^2 - 3B_1} \cos \gamma, \quad (\text{A11})$$

$$\text{with } \gamma \equiv \frac{1}{3} \cos^{-1} \left(\frac{2B_0^3 - 9B_1B_0 + 27K}{2\sqrt{(B_0^2 - 3B_1)^3}} \right).$$

Using the standard three flavour oscillation probability formula we can write the general expression for electron neutrino survival probability as

$$P_{ee} = 1 - 4 \sum_{j>k} \text{Re}|\tilde{U}_{ej}|^2 |\tilde{U}_{ek}|^2 \sin^2 \left(\frac{(\lambda_k - \lambda_j) L}{2} \right). \quad (\text{A12})$$

The expressions for the elements of the modified PMNS mixing matrix are given by

$$|\tilde{U}_{e1}|^2 = \sum_{i,j} U_{ei} U_{ej}^* S_{i1} S_{j1}^*, \quad (\text{A13a})$$

$$|\tilde{U}_{e2}|^2 = \sum_{i,j} U_{ei} U_{ej}^* S_{i2} S_{j2}^*, \quad (\text{A13b})$$

$$|\tilde{U}_{e3}|^2 = \sum_{i,j} U_{ei} U_{ej}^* S_{i3} S_{j3}^*, \quad (\text{A13c})$$

where we have defined

$$S_{i1} S_{j1}^* = \frac{\delta_{ij} \lambda_2 \lambda_3 - (H^{\text{vac}})_{ij} (\lambda_2 + \lambda_3) + (H^{\text{vac}2})_{ij}}{(\lambda_2 - \lambda_1) (\lambda_3 - \lambda_1)}, \quad (\text{A14})$$

$$S_{i2} S_{j2}^* = \frac{\delta_{ij} \lambda_1 \lambda_3 - (H^{\text{vac}})_{ij} (\lambda_1 + \lambda_3) + (H^{\text{vac}2})_{ij}}{(\lambda_1 - \lambda_2) (\lambda_3 - \lambda_2)}, \quad (\text{A15})$$

$$S_{i3} S_{j3}^* = \frac{\delta_{ij} \lambda_1 \lambda_2 - (H^{\text{vac}})_{ij} (\lambda_1 + \lambda_2) + (H^{\text{vac}2})_{ij}}{(\lambda_1 - \lambda_3) (\lambda_2 - \lambda_3)}. \quad (\text{A16})$$

From above Eqs. it is clear that we only need the eigenvalues of the modified Hamiltonian, H^{vac} in vacuum mass basis to get the analytical expression for P_{ee} . We also compute similar expressions when $\eta_{\tau\tau}$ is present as sNSI parameter and notice that we just need to interchange $s_{23} \longleftrightarrow c_{23}$ in the expressions for $\eta_{\mu\mu}$ to obtain the formula for $\eta_{\tau\tau}$.

-
- [1] Y. Fukuda *et al.* (Super-Kamiokande), *Phys. Rev. Lett.* **81**, 1562 (1998), [arXiv:hep-ex/9807003](#).
 - [2] Q. R. Ahmad *et al.* (SNO Collaboration), *Phys. Rev. Lett.* **89** (2002), [arXiv:0204008 \[nucl-ex\]](#).
 - [3] K. Eguchi *et al.* (KamLAND Collaboration), *Phys. Rev. Lett.* **90** (2003), [arXiv:0212021 \[hep-ex\]](#).
 - [4] P. A. Zyla *et al.* ((Particle Data Group Collaboration), *PTEP* **2020** (2020), 083C01.
 - [5] I. Esteban, M. C. Gonzalez-Garcia, M. Maltoni, T. Schwetz, and A. Zhou, *JHEP* **09**, 178 (2020), [arXiv:2007.14792 \[hep-ph\]](#).
 - [6] P. F. de Salas, D. V. Forero, S. Gariazzo, P. Martínez-Miravé, O. Mena, C. A. Ternes, M. Tórtola, and J. W. F. Valle, *JHEP* **2021** (2021), [arXiv:2006.11237 \[hep-ph\]](#).
 - [7] F. Capozzi *et al.*, *Phys. Rev. D* **101** (2020), [arXiv:2003.08511 \[hep-ph\]](#).
 - [8] B. T. Cleveland *et al.*, *Astrophys.J.* **496**, 505 (1998).
 - [9] F. Kaether, W. Hampel, G. Heusser, J. Kiko, and T. Kirsten, *Phys. Lett. B* **685**, 47 (2010), [arXiv:1001.2731 \[hep-ex\]](#).
 - [10] G. Bellini *et al.* (Borexino Collaboration), *Phys. Rev. Lett.* **107** (2011), [arXiv:1104.1816 \[hep-ex\]](#).
 - [11] K. Abe *et al.* (Super-Kamiokande Collaboration), *Phys. Rev. D* **83** (2011), [arXiv:1010.0118 \[hep-ex\]](#).
 - [12] B. Aharmim *et al.* (SNO Collaboration), *Phys. Rev. C* **88** (2013), [arXiv:1109.0763 \[nucl-ex\]](#).
 - [13] K. Abe *et al.* (T2K Collaboration), *Phys. Rev. Lett.* **124** (2020), [arXiv:1911.07283 \[hep-ex\]](#).
 - [14] K. Abe *et al.* (T2K Collaboration), *Phys. Rev. D* **103** (2021), [arXiv:2101.03779 \[hep-ex\]](#).
 - [15] M. Acero *et al.* (NOvA Collaboration), *Phys. Rev. Lett.* **123** (2019), [arXiv:1906.04907 \[hep-ex\]](#).
 - [16] M. Acero *et al.* (NOvA Collaboration), *Phys. Rev. D* **106** (2022), [arXiv:2108.08219 \[hep-ex\]](#).
 - [17] K. Abe *et al.* (Super-Kamiokande Collaboration), *Phys. Rev. D* **97** (2018), [arXiv:1710.09126 \[hep-ex\]](#).
 - [18] M. Aartsen *et al.* (IceCube Collaboration), *Phys. Rev. D* **91** (2015), [arXiv:1410.7227 \[hep-ex\]](#).
 - [19] B. Abi *et al.* (DUNE Collaboration), “Deep underground neutrino experiment (dune), far detector technical design report, volume ii: Dune physics,” (2020), [arXiv:2002.03005 \[hep-ex\]](#).
 - [20] K. Abe *et al.* (Hyper-Kamiokande Proto- Collaboration), *PTEP* **2015**, 53C02 (2015), [arXiv:1502.05199 \[hep-ex\]](#).
 - [21] K. Abe *et al.* (Hyper-Kamiokande Collaboration), *PTEP* **2018** (2018), [arXiv:1611.06118 \[hep-ex\]](#).
 - [22] S. Adrián-Martínez *et al.* (KM3NeT Collaboration), *J. Phys. G: Nucl. Part. Phys.* **43**, 084001 (2016), [arXiv:1601.07459v2](#).
 - [23] M. G. Aartsen *et al.* (IceCube Collaboration), *J. Phys. G: Nucl Part. Phys.* **44**, 054006 (2017), [arXiv:1607.02671 \[hep-ex\]](#).
 - [24] A. Fengpeng *et al.* (JUNO Collaboration), *J. Phys. G: Nucl. Part. Phys.* **43**, 030401 (2016), [arXiv:1507.05613](#).
 - [25] D. V. Forero, S. J. Parke, C. A. Ternes, and R. Z. Funchal, *Phys. Rev. D* **104**, 113004 (2021), [arXiv:2107.12410 \[hep-ph\]](#).
 - [26] C. A. Argüelles *et al.*, *Rept. Prog. Phys.* **83**, 124201 (2020), [arXiv:1907.08311 \[hep-ph\]](#).

- [27] C. A. Argüelles *et al.*, “Snowmass white paper: Beyond the standard model effects on neutrino flavor,” (2022), [arXiv:2203.10811 \[hep-ph\]](#).
- [28] L. Wolfenstein, *Phys. Rev. D* **17**, 2369 (1978).
- [29] B. Dev *et al.*, *SciPost Phys. Proc.* **2**, 001 (2019), [arXiv:1907.00991 \[hep-ph\]](#).
- [30] S.-F. Ge and S. J. Parke, *Phys. Rev. Lett.* **122**, 211801 (2019), [arXiv:1812.08376v2](#).
- [31] O. G. Miranda and H. Nunokawa, *New J. Phys.* **17**, 095002 (2015), [arXiv:1505.06254 \[hep-ph\]](#).
- [32] Y. Farzan and M. Tortola, *Front. in Phys.* **6**, 10 (2018), [arXiv:1710.09360 \[hep-ph\]](#).
- [33] K. Babu, G. Chauhan, and P. B. Dev, *Phys. Rev. D* **101** (2020), [arXiv:1912.13488v3](#).
- [34] C. Biggio, M. Blennow, and E. Fernandez-Martinez, *JHEP* **08**, 090 (2009), [arXiv:0907.0097 \[hep-ph\]](#).
- [35] T. Ohlsson, *Rept. Prog. Phys.* **76**, 044201 (2013), [arXiv:1209.2710 \[hep-ph\]](#).
- [36] S. K. Agarwalla, S. Das, M. Masud, and P. Swain, *JHEP* **11**, 094 (2021), [arXiv:2103.13431 \[hep-ph\]](#).
- [37] A. Kumar, A. Khatun, S. K. Agarwalla, and A. Dighe, *JHEP* **04**, 159 (2021), [arXiv:2101.02607 \[hep-ph\]](#).
- [38] M. Masud and P. Mehta, *Phys. Rev. D* **94**, 053007 (2016), [arXiv:1606.05662 \[hep-ph\]](#).
- [39] F. Capozzi, S. S. Chatterjee, and A. Palazzo, *Phys. Rev. Lett.* **124**, 111801 (2020), [arXiv:1908.06992 \[hep-ph\]](#).
- [40] I. Esteban, M. C. Gonzalez-Garcia, and M. Maltoni, *JHEP* **06**, 055 (2019), [arXiv:1905.05203 \[hep-ph\]](#).
- [41] E. Marzec and J. Spitz, *Phys. Rev. D* **106**, 053007 (2022), [arXiv:2208.04277 \[hep-ph\]](#).
- [42] A. N. Khan, W. Rodejohann, and X.-J. Xu, *Phys. Rev. D* **101**, 055047 (2020), [arXiv:1906.12102 \[hep-ph\]](#).
- [43] A. Y. Smirnov and X.-J. Xu, *JHEP* **12**, 046 (2019), [arXiv:1909.07505 \[hep-ph\]](#).
- [44] A. Medhi, D. Dutta, and M. M. Devi, *JHEP* **06**, 129 (2022), [arXiv:2111.12943 \[hep-ph\]](#).
- [45] A. Medhi, M. M. Devi, and D. Dutta, (2022), [arXiv:2209.05287 \[hep-ph\]](#).
- [46] T. Sarkar, (2022), [arXiv:2209.10233 \[hep-ph\]](#).
- [47] M. Agostini *et al.* (Borexino Collaboration), *Phys. Rev. D* **100**, 082004 (2019), [arXiv:1707.09279 \[hep-ex\]](#).
- [48] J. Venzor, A. Pérez-Lorenzana, and J. De-Santiago, *Phys. Rev. D* **103**, 043534 (2021), [arXiv:2009.08104 \[hep-ph\]](#).
- [49] P. B. Denton, A. Giarnetti, and D. Meloni, (2022), [arXiv:2210.00109 \[hep-ph\]](#).
- [50] L. Wolfenstein, *Phys. Rev. D* **17**, 2369 (1978).
- [51] J. Linder, (2005), [arXiv:hep-ph/0504264](#).
- [52] J. F. Nieves and P. B. Pal, *Am. J. Phys.* **72**, 1100 (2004), [arXiv:hep-ph/0306087](#).
- [53] C. C. Nishi, *Am. J. Phys.* **73**, 1160 (2005), [arXiv:hep-ph/0412245](#).
- [54] Y. Grossman, *Phys. Lett. B* **359**, 141 (1995), [arXiv:hep-ph/9507344](#).
- [55] B. Pontecorvo, *Sov. Phys. JETP* **6**, 429 (1957).
- [56] B. Pontecorvo, *Zh. Eksp. Teor. Fiz.* **34**, 247 (1957).
- [57] B. Pontecorvo, *Zh. Eksp. Teor. Fiz.* **53**, 1717 (1967).

- [58] P. A. Zyla *et al.* (Particle Data Group), *PTEP* **2020**, 083C01 (2020).
- [59] S. S. Chatterjee and A. Palazzo, *Phys. Rev. Lett.* **126**, 051802 (2021), [arXiv:2008.04161 \[hep-ph\]](#).
- [60] P. Coloma, *JHEP* **03**, 016 (2016), [arXiv:1511.06357 \[hep-ph\]](#).
- [61] A. de Gouvêa and K. J. Kelly, *Nucl. Phys. B* **908**, 318 (2016), [arXiv:1511.05562 \[hep-ph\]](#).
- [62] P. B. Denton, J. Gehrlein, and R. Pestes, *Phys. Rev. Lett.* **126**, 051801 (2021), [arXiv:2008.01110 \[hep-ph\]](#).
- [63] S.-F. Ge and S. J. Parke, *Phys. Rev. Lett.* **122**, 211801 (2019), [arXiv:1812.08376 \[hep-ph\]](#).
- [64] S.-F. Ge, *J. Phys.: Conf. Ser.* **1468**, 012125 (2020).
- [65] A. Ioannisian and S. Pokorski, *Phys. Lett. B* **782**, 641 (2018), [arXiv:1801.10488 \[hep-ph\]](#).
- [66] S.-F. Ge, K. Hagiwara, N. Okamura, and Y. Takaesu, *JHEP* **05**, 131 (2013), [arXiv:1210.8141 \[hep-ph\]](#).
- [67] P. Huber, M. Lindner, and W. Winter, *Comput. Phys. Commun.* **167**, 195 (2005), [arXiv:hep-ph/0407333](#).
- [68] P. Huber, J. Kopp, M. Lindner, M. Rolinec, and W. Winter, *Comput. Phys. Commun.* **177**, 432 (2007), [arXiv:hep-ph/0701187](#).
- [69] F. An *et al.* (JUNO), *J. Phys. G* **43**, 030401 (2016), [arXiv:1507.05613 \[physics.ins-det\]](#).
- [70] C. S. Fong, (2022), [arXiv:2210.09436 \[hep-ph\]](#).